DEVELOPMENT OF CHEMICAL SOLUTION DEPOSITED LEAD ZIRCONATE TITANATE FERROELECTRIC THIN FILMS FOR NON-PLANAR SUBSTRATES

by

Chloe Eileen Cook

A thesis submitted to the Faculty and the Board of Trustees of the Colorado School of Mines in partial fulfillment of the requirements for the degree of Master of Science (Materials Science).

Golden, Colorado

Date _____

Signed: _____
Chloe Eileen Cook

Signed: _____
Dr. Geoff Brennecka
Thesis Advisor

Golden, Colorado

Date _____

Signed: _____
Dr. Angus Rockett
Professor and Head
Department of Metallurgical and Materials Engineering

ABSTRACT

This thesis focuses on the development of a technique to deposit chemical solution derived thin films of the ferroelectric material lead zirconate titanate (PZT) onto non-planar substrates. PZT is a widely researched ferroelectric material for many thin film applications due to the magnitude of its dielectric, ferroelectric and piezoelectric properties. Chemical solution deposition (CSD) is a low cost, low capital method of depositing thin films which also allows for intimate mixing of precursors, leading to homogeneous final films. Applying CSD methods to non-planar substrates would allow for these quality films to be deposited on the three-dimensional structures which make up many devices that implement ferroelectric materials.

Ferroelectric PZT films were fabricated through a chelate route and deposited through both spin coating and dip coating methods. Conductive lanthanum nickelate (LNO) thin films were successfully created through a CSD method to be used as a bottom electrode for the PZT films. The PZT and LNO films on flat substrates were characterized through various techniques to verify their quality. Once quality films were achieved, the films could be applied to non-planar substrates.

Various methods of depositing chemical solution derived films onto non-planar substrates were explored and developed to account for specific material, size and processing constraints. The processes were optimized to deposit ferroelectric PZT films onto a specific silicon wedge substrate. Electron microscopy revealed that the techniques allowed for a successful deposition of the films onto the wedge substrate. These techniques could be applied to various non-planar substrates with similar constraints.

TABLE OF CONTENTS

LIST OF FIGURES AND TABLES

NOMENCLATURE

σ . . . . . applied stress

ε . . . . . strain

ε_r . . . . . relative dielectric constant

ε_0 . . . . . permittivity of vacuum

ρ . . . . . density

ω . . . . . angular velocity

η . . . . . viscosity

γ . . . . . surface tension

LIST OF ABBREVIATIONS

Lead zirconate titanate	PZT
Microelectromechanical systems	MEMS
Chemical solution deposition	CSD
Transmission electron microscopy	TEM
Iowa State University	ISU
Lanthanum nickelate	LNO
Morphotropic phase boundary	MPB
Metalloorganic deposition	MOD
Methoxyethanol	MOE
Sequential Precursor Addition	SPA
Inverted Mixing Order	IMO
Nuclear magnetic resonance	NMR
Fourier transform infrared spectroscopy	FTIR
Chemical vapor deposition	CVD
Atomic layer deposition	ALD
Field emission scanning electron microscopy	FESEM
X-ray diffraction/ diffractometer	XRD
Deionized	DI
Hydrogen fluoride	HF
2-butoxyethanol	2-BOE

ACKNOWLEDGMENTS

I would like to first and foremost thank my advisor, Dr. Geoff Brennecka, for his endless knowledge and patience throughout this process. His academic advice and guidance has helped set me up for an exciting career as a materials engineer and scientist. I would also like to thank my committee members, Dr. Meenakshi Singh and Dr. Ivar Reimanis for their expertise and willingness to assist me in my studies and beyond.

This work was helped along by undergraduate student, Lanie Breckenridge, who I commend for taking things into her own hands when I was not around and helping with much of the sample prep. Furthermore, the entire Functional Ceramics research group has been so welcoming and helpful, whether it is just commiserating over difficulty with data or help tweaking presentation slides. I am very grateful for their companionship, humor and wit.

Outside of Hill Hall, I would like to thank the my Mines cross country team for always being there throughout the stressful times, when all I needed was a run with friends to clear my mind. Finally, I am eternally thankful for the unconditional love and support from my family and fiancé, Grant, throughout my entire education here at Mines. Without them always reminding me of the bigger picture, I may not have gotten where I am today as smoothly as I have.

CHAPTER 1

INTRODUCTION

1.1 Publications

Some of the work discussed in this thesis has resulted in a publication in the ACS Applied Materials & Interfaces journal, with another in process[1]. The title of the publication is *In Situ TEM Study of the Amorphous-to-Crystalline Transition during Dielectric Breakdown in TiO_2 Film* was accepted to the journal on October 3, 2019. The techniques developed in this thesis were used to create samples that fit the constraints of the *in-situ* transmission electron microscope experiment. This specific *in-situ* setup required an electron transparent thin film of TiO_2 to be deposited onto a silicon sedge substrate so that dielectric breakdown could be observed in real-time. Although this publication focused on TiO_2 thin films, the rest of this thesis focuses on lead zirconate titanate thin films, which have slightly more complicated constraints than their TiO_2 counterparts. The untitled paper, in which the author of this thesis is a coauthor, that is currently in progress will focus on these more complicated thin films.

1.2 Introduction of Topics

The lead zirconate titanate ($PbZr_XTi_{1-X}O$, "PZT") system has been widely studied for its variety of ferroelectric properties that make it popular for many advanced electronic applications [2]. Some popular applications of PZT are nonvolatile random access memories, infrared detectors, microelectromechanical systems (MEMS), pyroelectric and piezoelectric sensors and far more which utilize its ferroelectric, piezoelectric and pyroelectric properties [3–6]. With the drive towards smaller, thinner and faster devices, the materials used in these applications must be researched in forms that would fit those requirements. Thin films of PZT material have been developed in many studies to satisfy size requirements as well as to optimize ferroic properties at those nano scales. For integration with semiconductor

devices, the need arises to deposit these films on non-planar surfaces to fit the structure of the device. While vapor deposition has been studied heavily for deposition of PZT into trenches and on varying topography, only a few studies have been conducted on chemical solution deposited PZT thin films onto non-planar surfaces [7–9]. This study investigates techniques to deposit PZT via chemical solution deposition (CSD) onto a particular non-planar silicon wedge substrate which in turn will be used for testing dielectric breakdown in-situ in a transmission electron microscope (TEM) in collaboration with Iowa State University (ISU). The setup of this experiment is shown in Figure 1.1 (a), along with the substrate geometry shown in Figure 1.1 (b). The requirements of this setup include the PZT film being thin enough to be electron transparent at the tip of the silicon wedge so that dielectric breakdown can be observed in real-time, as well as the PZT film being electrically contacted to the silicon substrate. The techniques developed in this study not only apply to this specific substrate, but to a wide range of non-planar substrates.

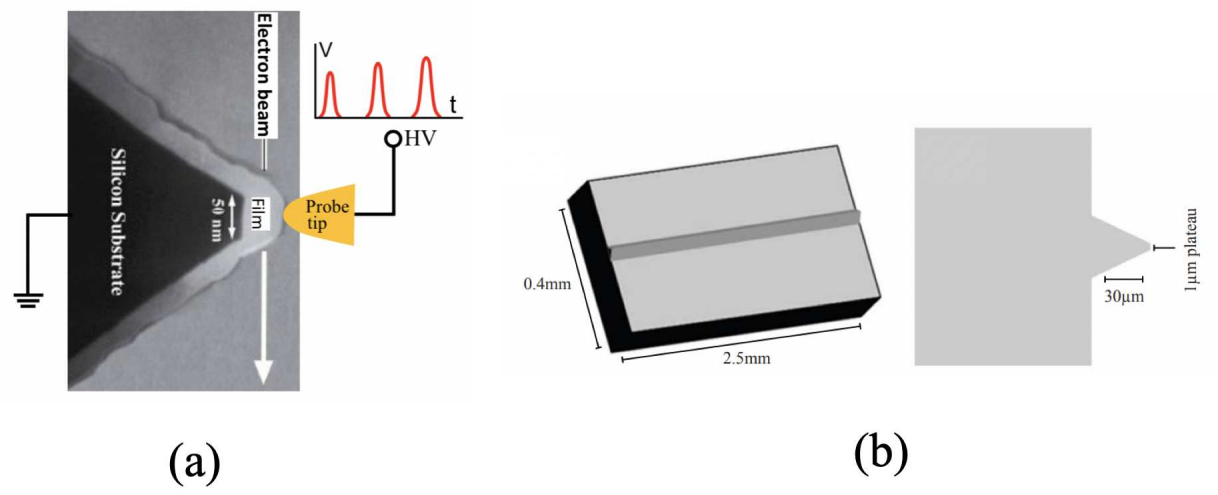

Figure 1.1: (a) TEM Experimental Setup(b) Substrate Geometry, PI 95 TEM PicoIndenter, obtained from Hysitron Product Literature.

The attractive ferroelectric properties of the PZT system arise from its perovskite structure, in which the Pb ions that sit on the corners of the unit cell are referred to as the A-site ions, and the Zr/ Ti ions which sit in the center of the unit cell are referred to as the B-site ions. These B-site ions displace along a crystallographic direction (e.g., <001> for tetragonal phase, <111> for rhombohedral), which creates a spontaneous polarization of the unit cell and leads to the ferroelectric domains observed in these materials. The composition of the PZT system significantly impacts the dielectric and ferroelectric properties of the material as well as its structure. The composition chosen for this study was a 52/48 ratio of Zr/Ti which sits on the morphotropic phase boundary of the material, between the tetragonal and rhombohedral phases at a large range of temperatures. This composition maximizes relevant properties, such as dielectric constant, piezoelectric constants and more, by a large amount compared to more Zr-rich or Ti-rich compositions [2].

Chemical solution deposition is a widely known route to creating PZT thin films, and provides many benefits compared to other methods, such as vapor deposition [10]. CSD is a low cost, low capital method for creating thin films that are reliable over large areas. This method uses low viscosity solvents which aid in intimate mixing of precursors at the molecular level, resulting in a homogeneous solution in a short period of time. Along with solution homogeneity, CSD allows for easy manipulation of composition, as the preparation time is very short and new solutions can be made in parallel with differing amounts of precursors.

This study explores the deposition of PZT onto non-planar surfaces, using a silicon wedge substrate as an example three-dimensional feature. Initial studies have been done on spin coating onto non-planar substrates, but faced challenges such as cracking and delamination [8, 9]. This study pursues dip coating as a method to achieve full, even coverage of the elevated features on non-planar substrates while not compromising the ferroelectric properties of the PZT [11]. While this work is applicable to a variety of non-planar substrates, there are a number of engineering constraints in place with the specific substrate dictated by the

collaborative project requirements. The substrate is a silicon wedge with a 1 μm plateau. The purpose of depositing PZT onto this type of substrate is to investigate the dielectric breakdown of a single grain of PZT on the tip of the wedge via an *in-situ* TEM setup. The first constraint of this substrate is that lead is highly reactive with silicon at elevated temperatures, such as those used for the crystallization step of the film, so a bottom electrode layer was required for the wedge substrate. A following constraint is that the PZT must be in electrical contact with the substrate for the *in-situ* experiment. While platinum is a common bottom electrode, it requires adhesion layers to attach it to silicon, which can pose difficulty in maintaining conductivity through to the silicon, which is required for the targeted *in-situ* TEM study. A conductive oxide that could be fabricated via CSD was determined to be the best option for full coverage of the substrate. Lanthanum nickelate ($LaNiO_3$, "LNO") was chosen due to the simplicity of the solution chemistry, the comparable lattice constant to PZT, and its conductivity. Another constraint posed by the substrate is the thickness at the wedge tip. For the TEM application, the film at the tip must be electron transparent in order for collaborators to observe dielectric breakdown. This required some alterations to the substrate itself as well as the dip coating process in order to achieve the end goal of a single, electron transparent grain on the tip of the wedge. Within these constraints, quality PZT films were fabricated through a CSD method. LNO films were also created through a simple CSD process. Once both films proved to have the necessary properties, various methods of dip coating were explored for the silicon wedge substrate.

CHAPTER 2

LITERATURE REVIEW

2.1 The Ferroelectric Lead Zirconate Titanate System

Piezoelectricity is defined as the ability of certain crystalline materials to develop an electric charge while under mechanical stress and was discovered in 1880 by the Curie brothers [2]. Considering the 32 point groups in which crystalline materials can fall, 21 are non-centrosymmetric, lacking a center of symmetry, and 20 can display piezoelectric properties. The piezoelectric effect can be described by the following equations:

Direct piezoelectric effect:

$$P_i = d_{ijk}\sigma_{jk} \tag{2.1}$$

Converse piezoelectric effect:

$$\varepsilon_{ij} = d_{kij}E_k \tag{2.2}$$

where in the direct effect, P is the polarization generated by applied stress, σ, and d is the piezoelectric coefficient, all acting in the specified *i, j* or *k* directions. In the converse effect, ε is the strain generated by the applied electric field *E,* and d is the same value piezoelectric constant as in the direct effect. These equations demonstrate the fact that piezoelectrics can have work done on them by their surroundings (direct effect) or do work on their surroundings (converse effect).

Within the 20 piezoelectric point groups, ten contain a unique polar axis which allows the crystal to display pyroelectricity, or the development of an electrical charge when uniformly heated. Ferroelectricity is a further subdivision of the pyroelectric point groups and is defined as the reversibility of the electric dipole when under an applied electric field [2].

These materials typically have a transition from a high symmetry, non-ferroelectric phase to their ferroelectric phase with some anisotropy below a temperature called the Curie point. This leads to a temperature dependent dielectric constant that obeys the Curie-Weiss law:

$$\varepsilon_r = \varepsilon_0 + \frac{C}{T - T_0} \tag{2.3}$$

where ε_r is the relative dielectric constant, ε_0 is the permittivity of vacuum, C is the Curie constant, and T_0 is the Curie temperature.

Materials in the Pb(Ti, Zr)O_3 solid solution system exhibit useful dielectric, piezoelectric, pyroelectric and ferroelectric properties that can be used in a variety of advanced electronic applications [3, 5, 6, 12].

2.1.1 PZT Phases and Structure

The PZT system takes on a perovskite crystal structure, which is a common structure of many ferroelectric materials. This structure is typically described as a simple cubic lattice with a large cation on the corners of the cube (A-site), and a smaller cation in the center of the cube (B-site), surrounded by an octahedron of oxygen atoms on each face center as shown in Figure 2.1. The octahedra of oxygen are each linked by the corners with the B-site cation filling the octahedral hole and the A-site cations filling the dodecahedral holes [2]. In PZT, the A-site cation is $Pb^{2+}$and the B-site cation is Zr^{4+}or Ti^{4+} randomly distributed through the unit cells according to the composition.

Spontaneous polarization in the perovskite structure occurs as the B-site cation displaces, causing the oxygen anions to displace opposite of the cation. While the perovskite structure is commonly shown as cubic, it can exist in many forms which are dictated by the direction of spontaneous polarization. For example, if the polarization arises from the B-site cation displacing in the <001> family of directions, the structure will elongate along that direction and in turn become tetragonal, where the the c/a ratio is greater than 1. If the B-site cation displaces in the <111> direction, the structure becomes rhombohedral.

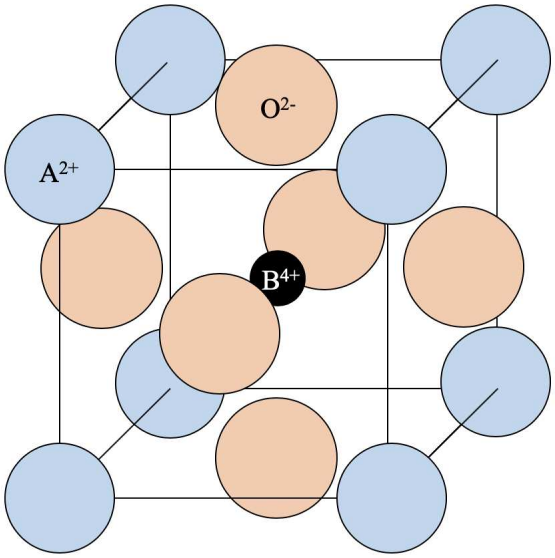

Figure 2.1: Example Cubic Perovskite Structure (not to scale).

In the PZT system, cubic, orthorhombic, monoclinic, rhombohedral or tetragonal perovskite structures can be formed depending on the composition and temperature [2, 13]. The sub-solidus phase diagram for the PZT system is shown in Figure 2.2. As shown, at room temperature more Ti-rich compositions will tend to form the perovskite structure with tetragonal symmetry, while more Zr-rich compositions form the perovskite structure with rhombohedral symmetry. At the composition of about 52% Zr, a morphotropic phase boundary (MPB) is observed. At this composition, the structure is fairly independent of temperature up to around 350°C, and is a mixture of the tetragonal and rhombohedral phases. In this work, the composition of PZT used is 52/48 Zr/Ti, right at the MPB, as this is the most common composition used for many applications.

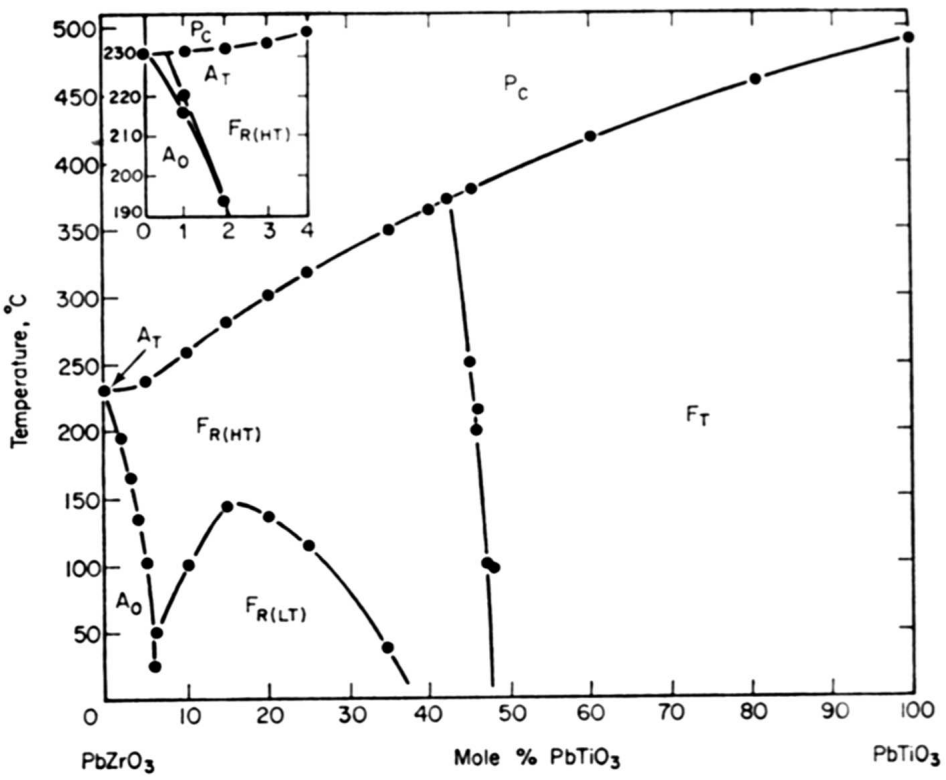

Figure 2.2: $PbTiO_3$- $PbZrO_3$ Sub-Solidus Phase Diagram [2].

2.1.2 PZT Ferroelectric Properties

PZT has highly composition dependent dielectric and piezoelectric constants that are maximized at the morphotropic phase boundary where these properties are relatively temperature independent, as shown in Figure 2.3. It is proposed that this arises from the increased ease of reorientation of the polarization axis. At this composition, the tetragonal and rhombohedral phases coexist, allowing for the six orientation directions of the tetragonal phase to be available along with the eight orientation directions of the rhombohedral phase, combining for a total of 14 orientation directions [2].

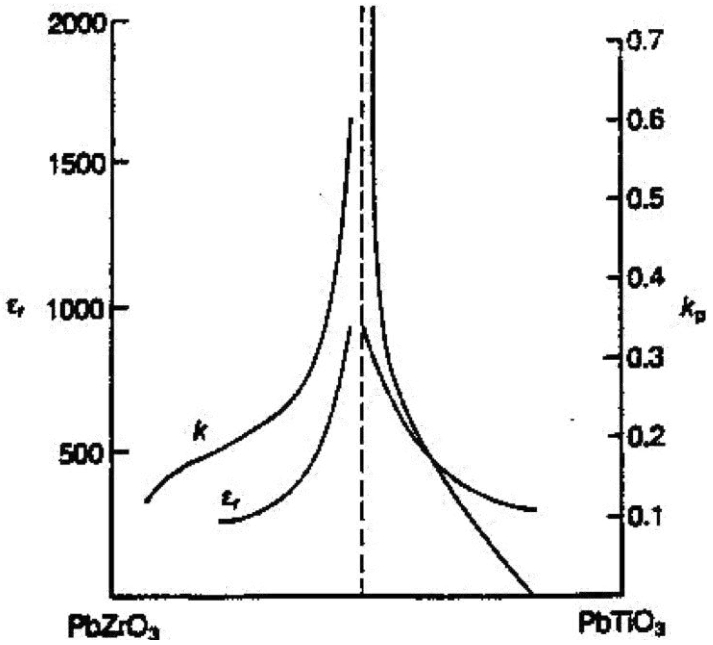

Figure 2.3: Dielectric and Planar Coupling Constant as a Function of PZT Composition [2].

Ferroelectric materials display hysteretic polarization vs. electric field (P-E) behavior, as shown in Figure 2.4. This behavior results from the presence of ferroelectric domains, defined as a volume in the material with complete alignment of electric dipoles [14]. The disordered boundaries between domains are referred to as domain walls, and they separate volumes of differing alignment. These domains can occur within a grain, where crossing a domain wall is not accompanied by a change in crystallographic alignment. Beginning with an unpolarized

material, if an electric field is applied, the ferroelectric domains will begin to switch within the constraints of the crystal structure to attempt to align with the field. This switching occurs by domain walls moving through the crystal as the domains align with each other. The relative dielectric constant (ε_r) can be found as one plus the slope of the curve $\left(\frac{\delta P}{\delta E}\right)$ at any point in the curve. By extrapolating the tangent line from the saturation point to the y-axis, the spontaneous polarization, P_s, can be found as the intercept, corresponding to the spontaneous polarization with all the dipoles aligned. Following the curve, if the electric field is removed, a ferroelectric material will retain some of its polarization, even at an electric field of E = 0. The finite value of polarization that remains is where the curve intersects the y-axis, and is called the remanent polarization, P_r. To return the net polarization to zero, an oppositely directed electric field must be applied at a strength of E_c, or the coercive field. At this point, the polarization of the dipoles reaches a net zero, and polarization can occur in this opposite direction if the strength of the electric field in that direction is increased. Factors such as composition, microstructure, temperature and others can affect the shape of these curves, and therefore the ferroelectric nature of the material.

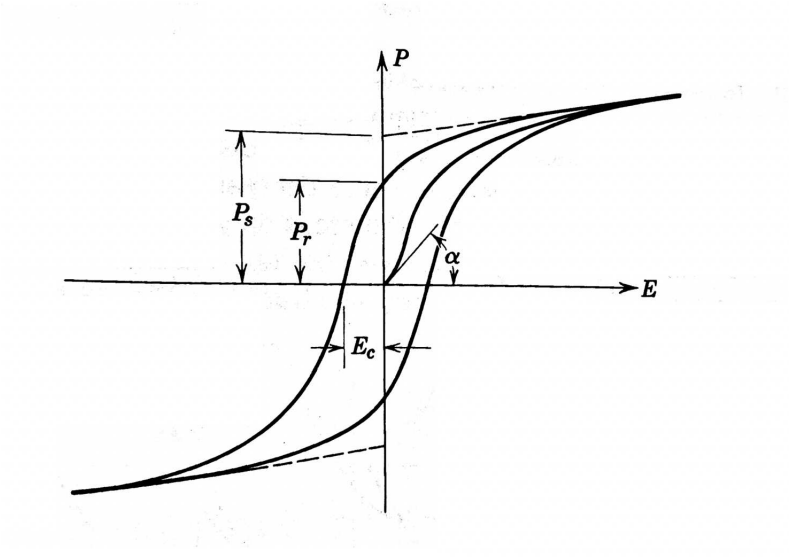

Figure 2.4: A Typical Ferroelectric Hysteresis Loop [14].

2.1.3 Thin Film vs. Bulk Ceramic Properties

Thin films often act differently than their bulk ceramic counterparts due to the fact that the microstructural and thickness dimensions begin to approach the length scales the properties of the film are governed by, such as ferroelectric domain size. When scaling down the physical dimensions of the material, these functional ferroelectric properties are typically suppressed due to intrinsic effects resulting from the larger fraction of surface atoms to bulk atoms. While these effects describe the fundamental size limits for stability of ferroelectricity, it is important to consider extrinsic effects that may not be inherent to the crystal itself. Thin films are severely impacted by the fact that they are essentially anchored to their substrate, while bulk materials are typically free standing. The substrate can impose both electrical and mechanical boundary conditions on the film, leading to effects such as electrode screening or external strain [15, 16].

Mechanical boundary conditions are important to consider when processing thin films, as they can result in altered ferroelectric properties. When a film is anchored to a substrate, a significant amount of strain can be induced in the film due to thermal expansion mismatch between the film and the substrate, stresses that occur during growth at the interface, and misfit in lattice parameters. These stresses can cause rearrangement in the domain structure, shift the Curie temperature and constant, and more effects which are not observed in bulk materials [17, 18]. The clamping of the grains at the interface to the substrate also limits the amount of switchable polarization that can occur in the interfacial layer [19]. In some cases, this low permittivity, non-ferroelectric "blocking" layer has been shown to impact the ferroelectric behavior of the films, and leads to a thickness dependence of properties such as the dielectric constant (ε_r), inverse coercive field (E_c) and remanent polarization (P_r). Multiple studies have found there to be no dependence of lattice constant or grain size on film thickness, but found ε_r and P_r to decrease and E_c to increase with decreasing film thickness [19–21]. While this blocking layer does affect ferroelectric properties, the presence of the layer is very dependent on processing conditions, and therefore can be controlled

and diminished, meaning the intrinsic ferroelectric properties of the films are not highly dependent on thickness.

Along with the clamping effect of substrates, growth from a substrate can be highly oriented and columnar in a thin film, while in a bulk ceramic the grain structure is more three-dimensional. The lateral size of columnar grains can approach the length scale of the thickness of the film, which can lead to grain to grain variations having an effect on properties of the film as a whole [16]. Substrates can have a significant effect on the ferroelectric properties of the films, and careful considerations must be made when choosing a substrate. These considerations will be discussed further in section 2.3.

2.2 Chemical Solution Deposition of Ceramic Thin Films

Chemical solution deposition (CSD) is a term used to describe processing in which precursor materials are dissolved in a solution and deposited onto a substrate to form a different material. CSD techniques have been studied dating as far back as 1935 [22], however the interest in depositing multicomponent oxide glasses, glass-ceramics and ceramics peaked throughout the next half a century [23–27] and further ramped up through the mid-1980's [10, 28–30] beginning with silica and simple oxide CSD systems. The benefits of CSD routes compared to other processing techniques such as glass melt routes and bulk powder processing drove further exploration of this method for many more complex material systems. The low viscosity solvents used in these processes allow for molecularly homogenous mixtures to be achieved quickly, which leads to homogenous material compositions once deposited. The synthetically created precursors used in these systems can be obtained in high purities compared to precursors obtained from minerals, which is important when considering the electronic properties that can be impacted by impurities. Finally, CSD routes can lead to lower processing temperatures due to the already intimately mixed precursors [31]. This allows films created through this method to be more easily integrated with metal and semiconducting substrates without concern for reactions that would proceed at higher temperatures. Many precursors and solvents will be mentioned in this section, so for ease

of the reader, Table 2.1 has been provided, with the chemical formulas associated with each chemical compound.

Table 2.1: PZT Solution Chemistry Precursors and Solvents.

Chemical Name	Chemical Formula	Type	Abbreviations
Lead (II) acetate trihydrate	$Pb(CH_3COO)_2{\cdot}3H_2O$	Precursor	$Pb(OAc)_2{\cdot}3H_2O$
Lead 2-ethylhexanoate	$C_{16}H_{30}O_4Pb$	Precursor	
Titanium isopropoxide	$Ti[OCH(CH_3)_2]_4$	Precursor	$Ti(OiPr)_4$
Titanium tetrabutoxide	$Ti(OCH_2CH_2CH_2CH_3)_4$	Precursor	$Ti(OBu)_4$
Zirconium acetylacetonate	$Zr(C_5H_7O_2)_4$	Precursor	
Zirconium butoxide	$Zr(OCH_2CH_2CH_2CH_3)_4$	Precursor	$Zr(OBu)_4$
Zirconium *n*-propoxide	$Zr(C_3H_8O)_4$	Precursor	
2-Methoxyethanol	$HOCH_2CH_2OCH_3$	Solvent	2-MOE
Methanol	CH_3OH	Solvent	MeOH
Acetic acid (glacial)	CH_3COOH	Chelating agent	HOAc

2.2.1 PZT Solution Chemistry

Within the CSD umbrella, there are many different solution routes that can be used to create the similar thin films. For the PZT system, three routes are commonly used: metalloorganic deposition (MOD), sol-gel, and chelate (commonly known as hybrid sol-gel). While MOD is the simplest route chemically, it has quite a few drawbacks that can be improved through the other two routes. The most common solution chemistry route for the PZT system is the sol-gel method using 2-methoxyethanol (MOE) as a solvent and chelating agent, developed by Budd *et al.* [30]. This work primarily uses the chelate route for creating PZT samples which was initially developed by Yi *et al.* [32] and further modified to the inverted mixing order chelate route by Assink and Schwartz [33]. Each route will be discussed in detail to develop an understanding of the benefits of each and why the inverted mixing order chelate route was chosen for this work.

2.2.1.1 Metalloorganic Decomposition

MOD involves the dissolution of metalloorganic precursors (such as titanium isopropoxide or titanium tetrabutoxide with zirconium acetylacetonate for the B-site, lead 2-ethylhexanoate

or lead acetate trihydrate for the A-site) into a solvent such as 2-n-butoxyethanol to create a simple solution in which no chemical reactions occur between the precursors [34, 35]. This route does not lead to the incorporation of multiple metal cations into a polymeric network, which eliminates the possibility of preferential cation pairing which has been known to influence the final reactions through which the solution goes to create the PZT thin film [36–38]. However, despite the success of some studies with this route, there are drawbacks to this method which led to it not being chosen as the main route in this study. First, while no chemical reactions between precursors is beneficial as described above, it also prevents a homogeneous solution from being formed, which could lead to gradients in composition and therefore ferroelectric properties, in the final film. Further, this method uses precursors and solvents that contain bulky organic compounds which must be burned out of the film at some point during processing. This leads to difficulty in creating crack-free films, as is noted by Sumi *et al.* and modifications must be made to avoid cracking.

2.2.1.2 Sol-Gel MOE Route

As noted, the sol-gel route using 2-MOE as a solvent is the most common method for creating quality PZT thin films. Sol-gel begins with alkoxide precursors that are dissolved in a solvent, and go through distinct hydrolysis and condensation steps, forming a polymeric gel. Budd *et al.* described the MOE method for thin films initially, and many works have used this original method with slight modifications as their synthesis route for PZT thin films [30, 39–44]. This method begins with metal-alkoxide precursors which are highly reactive with water, such as lead acetate trihydrate, titanium isopropoxide, and zirconium *n*-propoxide, or any other simple alkoxides of each precursor. The original procedure, shown in Figure 2.5, which is most commonly followed, proceeds according to three steps and works to remove as much water as possible through distillation to avoid the reactions that result in precipitation and condensation. The chemical reactions this method is based on are shown below, where M is the metal ion and R is the alkoxide group attached [45].

Hydrolysis:

$$M(OR)_x + H_2O \rightarrow M(OR)_{x-1}(OH) + ROH \tag{2.4}$$

Condensation (alcohol elimination):

$$2M(OR)_{x-1}(OH) \rightarrow M_2O(OR)_{2x-3}(OH) + ROH \tag{2.5}$$

Condensation (water elimination):

$$2M(OR)_{x-1}(OH) \rightarrow M_2O(OR)_{2x-2}(OH) + H_2O \tag{2.6}$$

Alcohol exchange:

$$M(OR)_x + xR'OH \rightarrow M(OR')_x + ROH \tag{2.7}$$

While this method is very reliable and versatile, it is more practical for large batches of single (or few) composition(s) of PZT due to the time cost of refluxing and distilling processes that could proceed over numerous days [46]. Another drawback of the MOE sol-gel method is the hazardous nature of the main solvent. 2-MOE is known to be a teratogen, carcinogen and mutagen, posing many health risks to the user and their offspring, and therefore not practical if other routes could be used for the processing.

2.2.1.3 Chelate Route

While distillation and refluxing are used in the MOE method to mitigate the reactions of the alkoxide precursors with water, there is another way to stabilize these precursors in air. This method is based on the chelation of the precursors, which involves replacing the reactive alkoxide groups with less reactive ligands, such as acetate groups. The main chelating agent used in these methods is acetic acid, which has been explored in a few different processing routes [32, 33, 48]. The main benefits of chelate routes are the simplicity of the

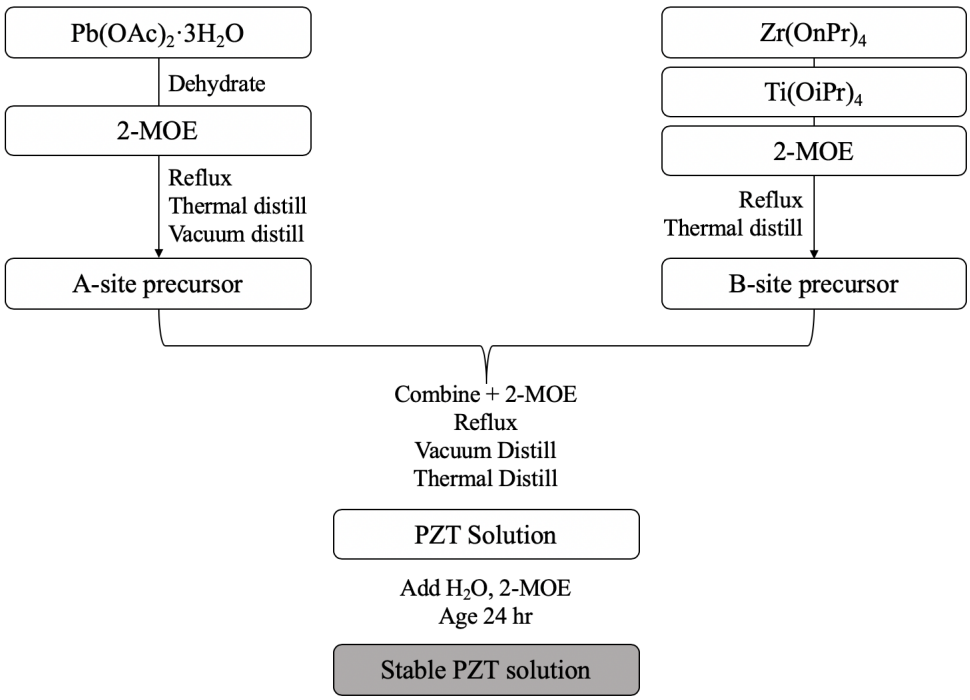

Figure 2.5: Flow Diagram for the MOE Solution Chemistry Method after Schwartz *et al.* [47].

solution processing, which makes it feasible to make many solutions of differing composition in parallel, as well as the use of more benign solvents compared to the MOE method. The reaction for chelation of a metal-alkoxide precursor by acetic acid is shown below.

$$CH_3COOH + M(OR)_x \rightarrow M(OR)_{x-1}(OOCCH_3) + ROH \tag{2.8}$$

Yi *et al.* developed a route commonly known as the sequential precursor addition (SPA) method [32]. This method begins with the dissolution of the lead acetate precursor in acetic acid followed by the addition of a zirconium alkoxide precursor and finally the titanium alkoxide precursor which are chelated by the acetic acid, creating a stable PZT system solution that is diluted with methanol (or a similar solvent) and more acetic acid. A flow diagram is shown for this method in Figure 2.6 (a). Assink and Schwartz developed another chelate route that improved solution homogeneity by chelating the B-site precursors with acetic acid first, then adding the lead acetate to the solution to dissolve [33, 49]. This method, referred to as the Inverted Mixing Order (IMO) method and shown in Figure 2.6 (b), is the method chosen for PZT solution synthesis in this work. Through the initial chelation of the zirconium and titanium precursors, more intimate mixing between the two can be achieved which leads to a homogenous film. The importance of the homogeneity of the film has been highlighted in a few studies, where the SPA and IMO methods were each used and the resulting film properties were directly compared. The IMO created films resulted in a higher remanent polarization, lower coercive field and more than doubled the dielectric constant compared to the SPA route [49]. Due to the use of acetic acid as both a chelating agent and solvent, this method is very simple in practice and relatively quick - requiring only minutes to hours compared to the multiple days that the MOE method requires.

While the fabrication of these chelate route PZT solutions may be simple, the chemical reactions through which they proceed are complex. Many studies have been performed to understand the modification of alkoxides by acetic acid, through nuclear magnetic resonance (NMR) and Fourier transform infrared spectroscopy (FTIR) [47, 50–54]. Through these

methods, three key reactions were found to occur: (1) exchange of alkoxide groups with acetate groups which releases free alcohols, (2) esterification, in which the "free" alcohols react with acetic acid to produce an ester and water, and (3) precipitation.

One drawback of the chelate routes that must be monitored is the aging process through which the solutions will proceed over time. This occurs due to the continued modification of the solution through esterification reactions. Free alcohol in the solution will continue to react with the acetic acid, which in turn produces more free alcohols [33]. Films produced from these aged solutions have shown inconsistent microstructure and ferroelectric properties. Boyle *et al.* investigated the time scale on which these processes occur and the effect that the aging had on film properties [55]. Although aging is seemingly unavoidable when using the IMO process, the simplicity of creating the solutions allows for fresh solutions to be made on a regular basis to produce films with consistent properties. One other consideration that must be made about this method is that the acetic acid-methanol system fails the Birnie test for rational solvent selection [56]. The vapor pressure and surface tension of each of the solvents are such that they are prone to creating striations across the film, resulting in varying thickness. If striations are noticeable on the films, methanol could be substituted for a lower vapor pressure solvents, such as butanol or toluene.

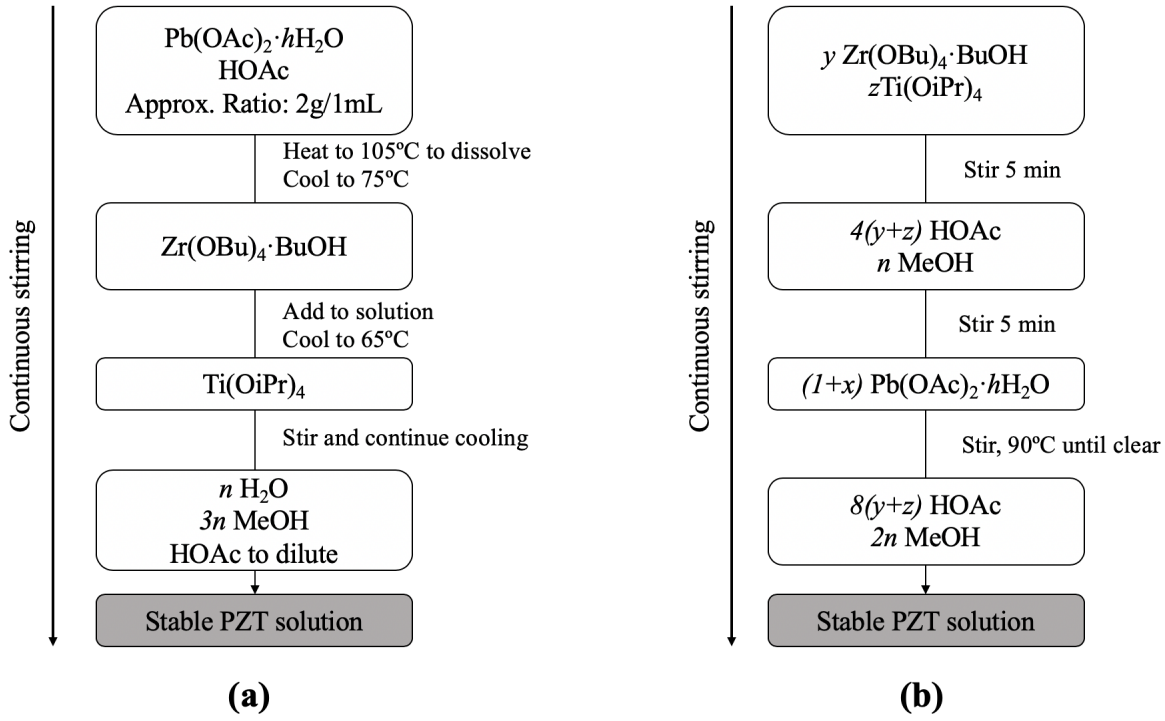

Figure 2.6: Flow Diagram for the Chelate Solution Chemistry Methods after Assink *et al.* [33].

2.2.2 Thin Film Deposition

Once the PZT solution is created, it is ready to be deposited onto a substrate through common methods such as dip coating, spin coating or spraying. Compared to vapor deposition, these CSD methods are inexpensive, require less equipment, and allow for precise control of microstructure (e.g., pore size, pore volume, surface area) and thickness [57]. The two methods that will be explored in detail in this work are spin coating and dip coating. Both methods rely on the same basic principles of fluid expulsion/ drainage and evaporation, and are followed by a pyrolysis step in which most of the organics in the film are removed before crystallization.

2.2.2.1 Spin Coating

Spin coating is a method used for flat, separate substrates that only require a film deposited on one side. This method creates very uniform films across the whole substrate surface, apart from corner and edge effects, for substrates ranging from small laboratory scale to industrial wafer scale. Bornside *et al.* described spin coating in four stages: (1) deposition, (2) spin-up, (3) spin-off, and (4) evaporation which are each depicted in Figure 2.7 [11]. While stages (1) and (2) can overlap, the first three steps generally follow a sequential order. Stage (4), evaporation, tends to occur throughout the whole process, which can cause issues if not monitored or mitigated in some way, so some precautions are taken to delay the start of evaporation [58].

The first step, deposition, involves depositing an excess of the precursor solution onto the substrate, either at a slow spin speed or no spin at all. The second stage occurs as the substrate begins its ramp up to its final speed, which is typically a few thousand revolutions per minute. During this stage, most of the fluid is pushed radially outward from the center of the substrate surface due to the centrifugal force caused by the spin rate. The third stage involves the remaining fluid to be pushed to the edge of the substrate, and ultimately expelled in the form of droplets from the surface. This stage leaves behind a thin and uniform film

of fluid on the substrate, which decreases in flow rate, as the thinner the film, the greater the resistance to flow [58]. The thickness uniformity developed in this stage arises from a balance of the centrifugal force, which forces the fluid radially outwards, and the viscous friction between the fluid and the substrate which drives the fluid radially inward [57]. As mentioned previously, the fourth stage begins concurrently with the other stages, but takes over as the main thinning mechanism once the film has thinned in the spin-off stage. Once the film cannot flow due to its thin nature, evaporation of the volatile solvent takes over and further thins the film until the whole process is complete. This leaves behind a film of any non-volatile precursors, namely the metal ions that are the basis of the film, and any organics that don't volatilize at room temperature. These organics are removed in a pyrolysis step that immediately follows the spinning process.

To directly affect the thickness and uniformity of the film, the spin-off stage is the most important stage to consider. The thickness (h) of the film is dependent upon spinning parameters (rotation speed, time at top speed, spin-up time), surrounding atmosphere (temperature, humidity), and solution properties (initial concentration, viscosity, solvent volatility). The thickness at any time t is described below:

$$h(t) = h_0 \cdot \left(1 + \frac{4\rho\omega^2 h_0^2 t}{3\eta}\right)^{-1/2} \tag{2.9}$$

where $h_0$is the initial thickness, ρ is the density of the liquid, ω is the angular velocity and η is the solution viscosity, assuming ρ and ω are constant [58, 59]. The spinning process creates a steady forced convection in the vapor above the substrate that causes the mass transfer coefficient, k, to be quite uniform, leading to uniformity in evaporation rate [57]. Once the film becomes too viscous to flow, evaporation takes over and brings the film to its final thickness. Meyerhofer *et al.* developed a model for the spinning process in which the spin-off and evaporation steps are separated [60]. This model gives a final thickness and elapsed time to achieve this thickness as:

$$h_{final} = \left(1 - \frac{\rho_0}{\rho}\right)\left(\frac{3\eta e}{2\rho_0\omega^2}\right)^{1/3} \tag{2.10}$$

$$t_{final} = t_{spin-off} + h_{spin-off}\left(\frac{\rho_0}{m\rho_A}\right) \tag{2.11}$$

where $\rho_A$is the density of the volatile solvent, ρ_0 is its initial value, and e is the evaporation rate that depends on the mass transfer coefficient, m [57]. Other models have been developed for sol-gel film deposition that account for evaporation overlapping the spin-off stage, among other factors [61].

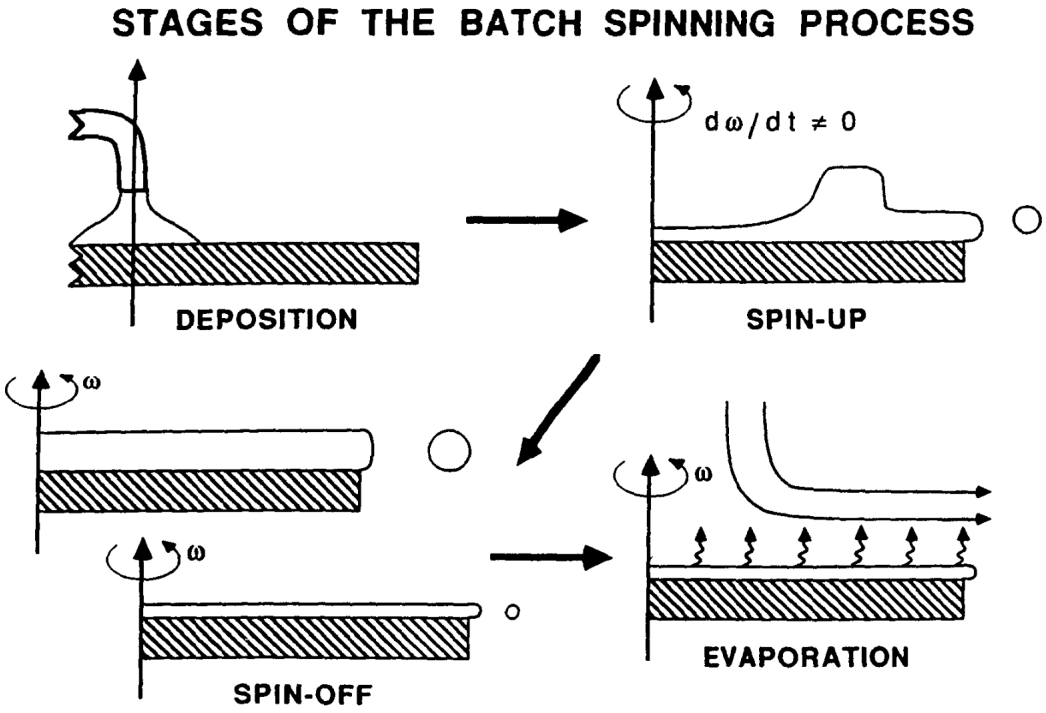

Figure 2.7: Four stages of the spin coating process [11].

2.2.2.2 Dip Coating

While spin coating can create denser and more uniformly thick films, dip coating has advantages when it comes to certain shape substrates [57]. Dip coating is best used when a

process requires a substrate that needs all surfaces coated with the film, or has protruding surfaces that must be uniformly coated. As with spin coating, dip coating can be broken into stages, which were initially described by Scriven, and shown in Figure 2.8: immersion, start-up, deposition, drainage and evaporation [58]. Using volatile solvents, such as the ones used in the PZT CSD system, evaporation tends to accompany the start-up, deposition and drainage steps. The continuous dip coating process, shown in Figure 2.8f, separates immersion from the other stages, eliminates start-up and "hides" drainage in the deposited film [57]. A competition among six different forces determines the thickness and uniformity of the dip coated film. The main forces in question are viscous drag by the substrate on the liquid, gravity, surface tension in the concavely curved meniscus, inertial forces of the boundary layer of liquid arriving at the substrate surface, surface tension gradient and disjoining/ conjoining pressure [58].

The thickness *(h)* of the film when solution viscosity (η) and withdraw rate (U) of the substrate are sufficiently high enough to reduce the curvature of the meniscus is described below [58, 62]:

$$h = c_1 \left(\frac{\eta U}{\rho g} \right)^{1/2} \tag{2.12}$$

where $c_1$is the proportionality constant, and has been experimentally shown to be 0.8 for Newtonian liquids [62]. This model shows that viscous drag, $\frac{\eta U}{h}$, and the force of gravity, $\rho g h$, are in balance under those conditions. Conversely, when solution viscosity and withdraw rate are not high enough to remove the meniscus curvature, which is common in sol-gel processes, the equation for thickness becomes:

$$h = 0.944 \left(\frac{\eta U}{\gamma_{LV}} \right)^{1/6} \left(\frac{\eta U}{\rho g} \right)^{1/2} \tag{2.13}$$

where γ_{LV} is the liquid-vapor surface tension. In this scenario, a third force is introduced, and the ratio of viscous drag to the surface tension is included in the calculation [58]. The

parameters that are most commonly changed to alter thicknesses in dip coating processes are solution viscosity/ concentration and withdrawal rate.

Dip coating requires a lower concentration solution than spin coating to achieve the same film thicknesses, as it does not involve forceful expulsion of fluid as in spin coating. Other considerations that must be made when dip coating are the size and shape of the substrate, as meniscus effects can alter the thickness at the bottom of the substrate.

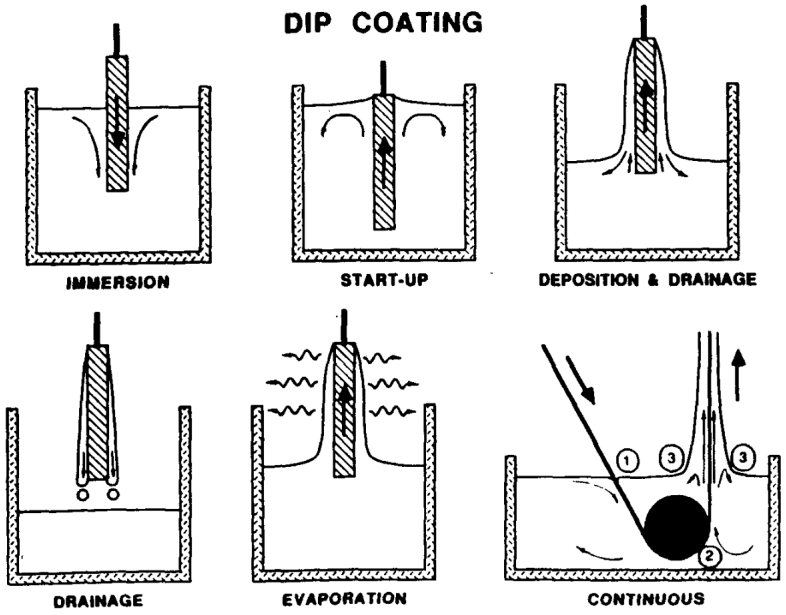

Figure 2.8: Stages of the dip coating process [58].

2.2.3 Post-Deposition

Once the PZT films are deposited, they still retain a significant organic fraction despite the evaporation that occurs during deposition. A pyrolysis step is used to remove a majority of the organics. Pyrolysis is typically achieved at temperatures between 200°C - 400°C, and results in an amorphous film that shrinks to 50-70% of its as-deposited thickness [45]. The shrinkage leads to two main results: increased concentration of the precursors in the film, and significant tensile stresses within the film and at the interface with the substrate. These stresses can in many cases leads to cracking of the film [45]. The extent of the stresses, and

whether or not cracking will occur can be dependent on the reactivity of the precursors, with less reactive precursors forming a solid film slowly, and therefore allowing time for the solvent to evaporate without causing much stress. Multilayering with pyrolysis steps in between each layer can also reduce the chances of cracking while still achieving the thicknesses needed. The addition of multiple thinner layers to create a film also reduces the chance of pinholes through the entire film that could cause shorts to occur between the top and bottom electrodes.

2.2.4 Crystallization of Films

Following pyrolysis, the amorphous PZT films are converted into a polycrystalline perovskite film. Crystallization steps can be performed in between each layer deposited, or following all layer depositions. It has been reported that around the morphotropic phase boundary of PZT, the amorphous thin film will crystallize first into a fine-grained metastable fluorite or pyrochlore phase around 500°C before reaching equilibrium in the perovskite structure once the final crystallization temperature is reached [43, 63–66]. Brooks *et al.* originally studied the how the pyrolysis condition affected this intermediate phase in thin films, finding that under oxidizing conditions the pyrochlore phase was actually stabilized, slowing the transition to the perovskite phase [43]. Tuttle *et al.* explored this phenomena further using transmission electron microscopy to observe the microstructural evolution of the films through pyrolysis and crystallization [64]. In this study, it was found that the intermediate phase actually consisted of two interpenetrating nanocrystalline phases, one being the pyrochlore phase, and one being a lead-deficient, zirconium rich amorphous phase. Upon further heating to temperatures around and above 650°C, the perovskite phase is reached and observed in two forms: (1) large "rosette" structures on the order of 2μm embedded in a fine grained matrix, and (2) dense equiaxed particles on the order of 100nm. The proposed mechanisms of this crystallization begins with phase separation in solution, followed by crystallization of the pyrochlore phase, which further results in heterogeneous nucleation of the final perovskite phase and finally homogeneous nucleation of the perovskite phase. This crystallization path was confirmed through *in-situ* diffraction experiments performed

by Nittala *et al.,* where the pyrochlore phase was shown to appear around 500°C. and disappeared upon the initial formation of the perovskite phase around 650°C [67]. It is important to understand the role of pyrochlore in the phase transformation of PZT, as it can severely impact the ferroelectric properties of the material. To avoid any remaining pyrlochlore, heating to temperatures above 650°C is important when creating high quality ferroelectric films.

2.3 Substrate Considerations

As mentioned previously, the substrate used in thin film processing can have a large impact on the ferroelectric properties of the film. The type of substrate can also alter the processing methods through which films are created. This section will discuss the specific substrates used in this work and the considerations that need to be made for their integration with PZT thin films.

2.3.1 Deposition on Non-Planar Substrates

Almost all devices on which PZT could be integrated, especially microsensors and microactuators, possess some sort of structural features that are not planar with the surface. Patterned oxide layers in these devices have typically been formed by uniform film deposition followed by a chemical or ion etch. While this is an effective method, it requires large capital expenses, as well as multiple steps in the process, including deposition, photolithography and patterning and the etch. A deposition method that evenly deposits on all surfaces without compromising the dielectric properties would reduce the process to only a deposition step. For simple oxide layers, this has been done very successfully at the research and industry level through chemical vapor deposition (CVD) and atomic layer deposition (ALD). ALD is extremely good at evenly coating three-dimensional features on substrates due to self-limiting reactions. For PZT, studies have been done into using ALD to deposit extremely uniform films onto non-planar surfaces with some success, however, many difficulties still arise in controlling stoichiometry and dielectric properties of these films [68–71].

Other methods that have been explored for depositing PZT thin films on three-dimensional structures include spray coating [72] and electrophoretic deposition [73].

As mentioned in previous sections, CSD has proven to improve homogeneity in stoichiometry for PZT thin films as well as enhanced dielectric properties compared to vapor deposited films. The challenge of obtaining a uniform PZT film on three-dimensional features through CSD has been pursued by a few groups. Mikalsen *et al.* used monolayer mediated patterning, which involved microcontact printing of a pattern, then spin coating onto a patterned surface followed by a lift-off step. Another route used in the aforementioned study was micromold-mediated patterning, which utilized capillary action to infiltrate a pattern with the precursor solution [9]. Both of these methods involve directed deposition as well as the creation of a compatible patterned surface. Cooney *et al.* used spin coating to deposit PZT solutions onto substrates with elevated surface features, showing difficulties with cracking and delamination of the films when the ratio of film thickness to step height was low (<0.35) [8]. To reduce the cracking, multiple thinner layers were deposited to obtain the desired thickness. While these initial studies have been done for PZT solution deposition onto nonplanar substrates, there is still much room to develop a deposition method that creates a uniform film on elevated features, minimizes macro-defects such as cracking, particle inclusions and delamination, as well as retains the enhanced properties that PZT possesses. This work looks to fill in the gaps in this area by developing a method for deposition of chemical solution derived films onto a non-planar silicon wedge substrate. The methods used in this study could be further applied to other non-planar, complex substrates.

2.3.2 PZT on Silicon

When considering the type of substrate on which to deposit PZT thin film layers, not only should the ferroelectric film properties not be degraded by the substrate, but it is also important to consider the any detrimental effects to the substrate itself. Because these films eventually will be integrated in devices with multiple layers below them, they must not compromise the underlying device characteristics. Silicon is the main component of many

semiconductor devices, however, the volatility of PbO and the interdiffusion of Pb and Si into the substrate can lead to conduction through areas required to be electrically isolated by the thin film as well as delamination [74]. In thick films on silicon substrates, sintering aids were studied to combat this issue by reducing temperatures necessary [75]. Possibly the most widely used method to combat the Pb-Si interdiffusion is the deposition of a diffusion blocking boundary layer between the Si and PZT interface [76, 77]. These layers vary from platinum adhered with adhesion layers, TiN_x, ZrN_x, TiO_x and more. In this work, for initial studies of PZT, platinized silicon substrates were used where Pt was adhered with silica and titania adhesion layers.

2.3.3 $LaNiO_3$ as a Bottom Electrode

The wedge substrates used in this study are silicon, with no diffusion blocking boundary layers. This leads to the necessity of a bottom electrode layer that successfully blocks the diffusion of Pb into the silicon, and also can be easily deposited and adhered to the silicon wedge. Platinum has been shown to cause fatigue in PZT remanent polarization, so recently many studies have been conducted to replace platinum as a bottom electrode with $LaNiO_3$ (LNO), a conductive oxide that can be easily solution deposited and has a matching lattice constant to PZT [78–82]. Meng *et al.* proposed that the LNO acts as a sink for oxygen vacancies, reducing electron trapping and therefore leading to less domain pinning which would cause the remanent polarization to decrease with repeated cycles (ferroelectric fatigue) [80]. In the case of this work, there is also a difficulty maintaining conductivity through the adhesion layers that would be necessary for Pt to be used as a bottom electrode. (1 0 0) textured LNO films, which template to the (1 0 0) Si substrate, have shown closely matched lattice parameters to PZT ($a_0 = 0.384$nm for LNO oxygen sublattice to $a_0 = 0.405$nm for PZT oxygen sublattice) [78, 83, 84]. Along with a matched lattice constant, LNO also exhibits a perovskite-like structure, close to that of PZT. The conductive nature of LNO makes it a suitable bottom electrode for PZT, with a low resistivity on the order of $1\text{x}10^{-3}\Omega$cm at room temperature [78–81]. In the studies referenced, the PZT films deposited on the LNO

substrates displayed a (1 0 0) texturing and also comparable ferroelectric properties to PZT films deposited on other traditional substrates.

2.3.3.1 LNO Solution Chemistry

One of the main drawbacks of using the traditional platinum bottom electrode for this study is the difficulty of getting the platinum to stick to the silicon substrate. On typical flat substrates, adhesion layers of silica and titania are used to keep the platinum from peeling off of the silicon. For the wedge/ non-planar substrates used, the addition of these adhesion layers as well as the sputtering of the platinum onto the substrate would present great difficulties and more capital intensive processes. LNO was chosen as a bottom electrode partially because of its simple solution chemistry for CSD processes, and the fact that it can be deposited with the same methods used for the PZT films. LNO solutions have typically been created through simple MOD processes involving two miscible solvents and the lanthanum nitrate ($La(NO_3)_3$) and nickel acetate ($Ni(CH_3COO)_2$) precursors [78–81]. Solvents such a 2-MOE, acetic acid and water have been used, but any solvents that are miscible in each other, dissolve the precursors, and pass the Birnie test of vapor pressure and surface tension could be suitable [56]. These solutions, once deposited typically go through a pyrolysis step around 400°C and a subsequent crystallization step from 600-700°C. As a bottom electrode, the most important properties of the LNO film are full coverage of the substrate, to remove the possibility of pinholes that cause shorts and a low resistivity. The electrical properties of LNO are not severely impacted by off-stoichiometry or cation clustering, and therefore the solution chemistry is not as crucial to control as with PZT.

CHAPTER 3

LEAD ZIRCONATE TITANATE THIN FILMS

3.1 Motivation and Constraints

To develop a technique for depositing ferroelectric PZT thin films on non-planar substrates, quality chemical solution deposited PZT thin films must first be fabricated and characterized. In this study a "quality" PZT films are defined to possess the following: continuity, uniform thickness, a crystalline perovskite structure, and ferroelectric characteristics. Continuity is important, as the film must cover the entire substrate and display consistent properties throughout without the presence of cracks. It is also important to consider that even if the film appears continuous to the naked eye, pinholes in the film can be present and cause shorts from the top electrode to the bottom electrode. Uniform thickness is important, because as discussed in section 2.1.3, the ferroelectric properties can be dependent on thickness. The film must be fully crystalline and not contain any second phases that would degrade properties, such as pyrochlore. Finally, the film must be able to display ferroelectric behavior when subjected to an electric field to be defined as a "quality" film.

3.2 Preparation of PZT Thin Films

3.2.1 Substrate Preparation

For deposition of PZT films, a flat platinized silicon substrate ($Pt/Ti/SiO_2/Si$) that was cleaved into small rectangular pieces was used. These substrates were created by and obtained from the Army Research Laboratory. These substrates were chosen as example flat substrates for the PZT films, and used for preliminary testing of the PZT properties. Although platinum is not the bottom electrode that is be used for the silicon wedge substrate, the PZT properties will remain the same regardless of substrate. Each substrate was cleaned by spinning methanol at 4000 rpm for 30 seconds on the substrate, and dusted with N_2 gas to remove any remaining particulates. These substrates were used as an example flat substrate

so characterization could be carried out to determine if the PZT films were quality before exploring methods to deposit on the silicon wedge substrate.

3.2.2 PZT Thin Film Solution Deposition

The solution synthesis for the PZT films was conducted based on the IMO process developed by Assink and Schwartz [33]. All solution preparation, deposition, drying and pyrolysis steps were performed in a fume hood, as the IMO method does not require a highly controlled environment. Zirconium (IV) butoxide, $Zr(OBu)_4$ (80wt% in 1-butanol, Sigma Aldrich) was first added to a glass vial, followed by titanium (IV) isopropoxide, $Ti(OiPr)_4$ (>97.0%, Sigma Aldrich) in amounts to achieve the 52/48 Zr/Ti composition. Glacial acetic acid, HOAc (Fischer Scientific) was added to the B-site precursors in a ratio of 10 moles HOAc per cation to chelate the solution and prevent against hydrolysis. This solution was mixed for 5 minutes, and then methanol, MeOH, was added to dilute. Lead (II) acetate trihydrate, $Pb(OAc)_2$ (>99%, Sigma Aldrich) was added in 10% excess stoichiometry to account for volatility of PbO at high temperatures. This solution was heated at 90°C while stirring to dissolve the lead acetate precursor. Once the solution was clear, and all solids dissolved, it was removed from heat and methanol was added to cool and dilute. Acetic acid was added once the solution had cooled to further dilute the solution to its final concentration of 0.35 moles per liter (0.35M).

To spin coat the films, the solutions were collected in a syringe and passed through a 0.45μm filter to remove any large particulates. The solution was statically dispensed onto the cleaned substrate in an MTI Corporation VTC-100 spin coater. The substrate was immediately spun at 4000 revolutions per minute for 30 seconds. A pyrolysis step followed the spin deposition on a hot plate at 400°C for 1 minute to remove most of the organics and then cooled through contact with a room temperature surface. The spin/ pyrolysis steps were repeated up to four times to achieve the final desired thickness. Following pyrolysis, crystallization was performed at 700°C in a box furnace for 10 minutes.

Once the films were crystallized, top electrodes were deposited by evaporation through a mask with 0.004 inch (100μm) diameter holes. Copper and gold electrodes were used in this study due to the availability and ease of their evaporation.

3.3 Characterization Techniques

3.3.1 Film Thickness

Film thickness was characterized by two techniques: profilometry and field emission scanning electron microscopy (FESEM). For profilometry, a small section of the film was etched out using a BOE etchant to create a step-edge from the top of the film to the substrate. A Dektak Profilometer was used to measure across a 1mm section which encapsulated the step edge. This method reports the height changes within the 1mm section, and a thickness was calculated by subtracting the initial height (on the etched out portion) from the final height which would include the film.

To measure the thickness with FESEM imaging, a PZT thin film sample was cleaved, coated in sputtered gold, and mounted so that the cross-section could be imaged. A JEOL 7000 field emission electron microscope was used in secondary electron imaging mode with a 20.0kV accelerating voltage. The imaged cross section was measured to determine the thickness, and this measurement was compared to those obtained with the profilometer.

3.3.2 Structural and Microstructural Characterization

To verify the perovskite structure of each film, a PANalytical PW3040 X-ray Diffractometer (XRD) with Bragg-Brentano geometry and Cu-Kα radiation was used. Scans were conducted from 2θ angles of 20° to 60°. To determine the microstructure of the films and verify crystallinity, a JEOL 7000 field emission electron microscope was used in secondary electron imaging mode with a 20.0kV accelerating voltage. Due to the dielectric nature of the PZT, the films had to be coated in sputtered gold in order to be imaged without charging effects in the FESEM.

3.3.3 Ferroelectric Measurements

Ferroelectric measurements were made using the Radiant Technologies Precision Materials Analyzer. A probe station was setup specifically for thin film ferroelectric measurements, and is shown in Figure 3.1. One probe was contacted to a top electrode, and the other was contacted to either a shorted top electrode or the bottom electrode if it was exposed. Voltages varying from 10V to 30V were applied in the positive and negative directions and polarization was measured based on the electrode area.

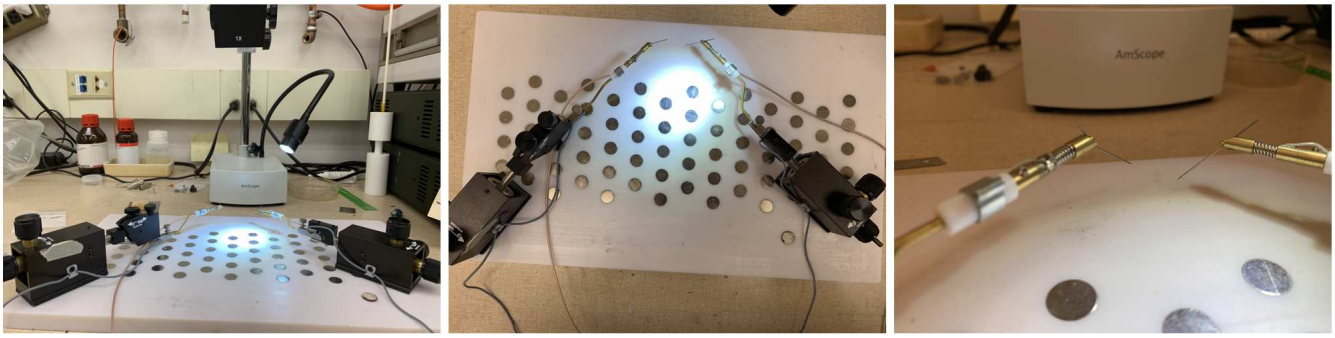

Figure 3.1: Probe Station Setup for Ferroelectric Measurements.

3.4 Results and Discussion

3.4.1 Visual Film Quality

Early experiments with the CSD process in this study led to films with cracks that were observable to the naked eye. Cracks were observed to occur directly after pyrolysis or during crystallization, shown in Figure 3.2. In Figure 3.2 (a), it is also readily apparent that the thickness was uneven throughout the film, based on the gradient in color. This was persistent in some of the early films, caused by either particles on the surface that inhibited the smooth evening out of the film, or from the viscosity of the solution being too high to thin out evenly when being spun. These samples cracked at some point during crystallization in the furnace after all four layers were deposited, which could have been caused by the organic chains not being completely removed during pyrolysis. The crystallization step involves the film

being directly subjected to 700°C, and the rapid increase in temperature could have caused the organics to immediately burn out, causing cracks in the film on their way. The cracks formed in Figure 3.2 (b) formed during a pyrolysis step in between layers three and four, which points to the cause being the thickness of each layer.

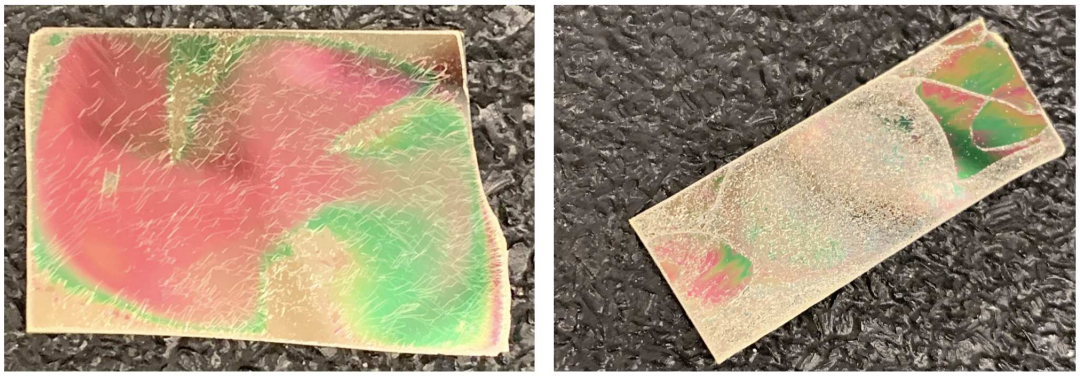

Figure 3.2: Example Cracked PZT Films: (a) Cracks Formed During Crystallization (b) Cracks Formed During Pyrolysis.

Multiple steps were taken to combat the cracking, and the above procedure is the final process used that resulted in crack-free films. The first change that was made was extending the pyrolysis time from 30 seconds to 1 minute in order to remove more of the organic content. It was thought that upon crystallization, many organics still needed to leave the film and at high temperatures, such as 700°C, this occurred rapidly, causing cracks in the films. The next step taken was reducing the molarity of the solution in order to reduce the thickness of the deposited film as well as the clumping of organic chains in the film. The molarity was reduced from 0.4M to 0.35M. The final step taken to reduce cracking was eliminating any time between deposition and spinning. Due to a lag in the program of the spin coater, the solution had previously been sitting on the substrate for 10 seconds before spinning began. With a timer, the solution was dispensed at the end of this lag time to avoid any evaporation from occurring before spinning, which would lead to thicker films that cracked more easily. These changes in the process led to crack-free, uniform thickness films. Figure 3.3. shows

an example quality film, with very little variation in color, and therefore thickness, and no visible cracks. These changes were implemented and used for any further PZT processing.

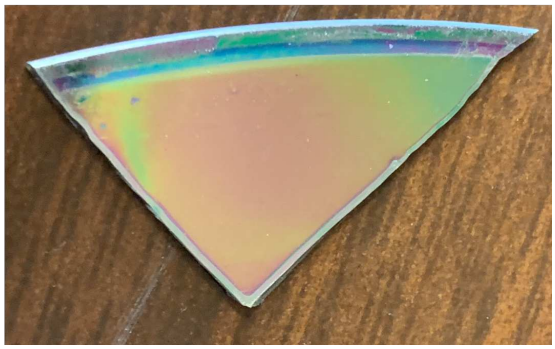

Figure 3.3: Example Quality PZT Film.

3.4.2 Film Thicknesses

Film thicknesses were measured on films from one to four layers of spin coated PZT, where a layer is defined as one deposition of film. Thicknesses of 115±5nm (statistical error) per layer were recorded through profilometry. This was consistent and thickness varied linearly with the amount of layers of PZT film deposited with an R^2 value of 0.9957, as shown in Figure 3.4.

This result shows that thickness was directly related to the number of layers, and was easily tunable. A cross sectional FESEM image was also obtained of the PZT films, shown in Figure 3.5. A thickness of ∼350nm for the three layer PZT sample is found, which is consistent with the profilometry findings. The cross section also displayed a columnar grain structure, which is expected from a CSD film on (111) platinum.

3.4.3 Crystallinity and Microstructure of PZT Films

The perovskite structure was verified through XRD for the PZT films. Figure 3.6 shows the XRD pattern for a three layer PZT film deposited from a solution with 10% Pb excess. A clear perovskite pattern can be seen with the presence of a PbO peak. The sharpness of this peak indicates large PbO crystallites sitting on the surface of the film. This peak was present

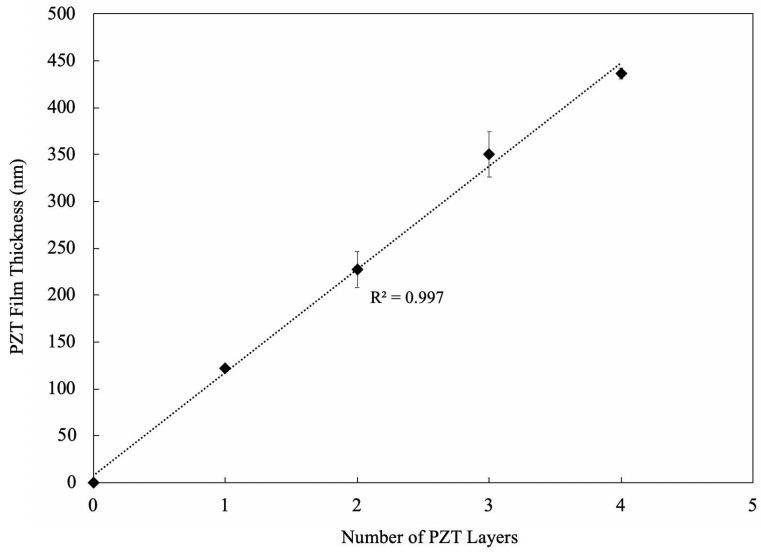

Figure 3.4: Thickness of PZT Films as a Function of Number of Layers.

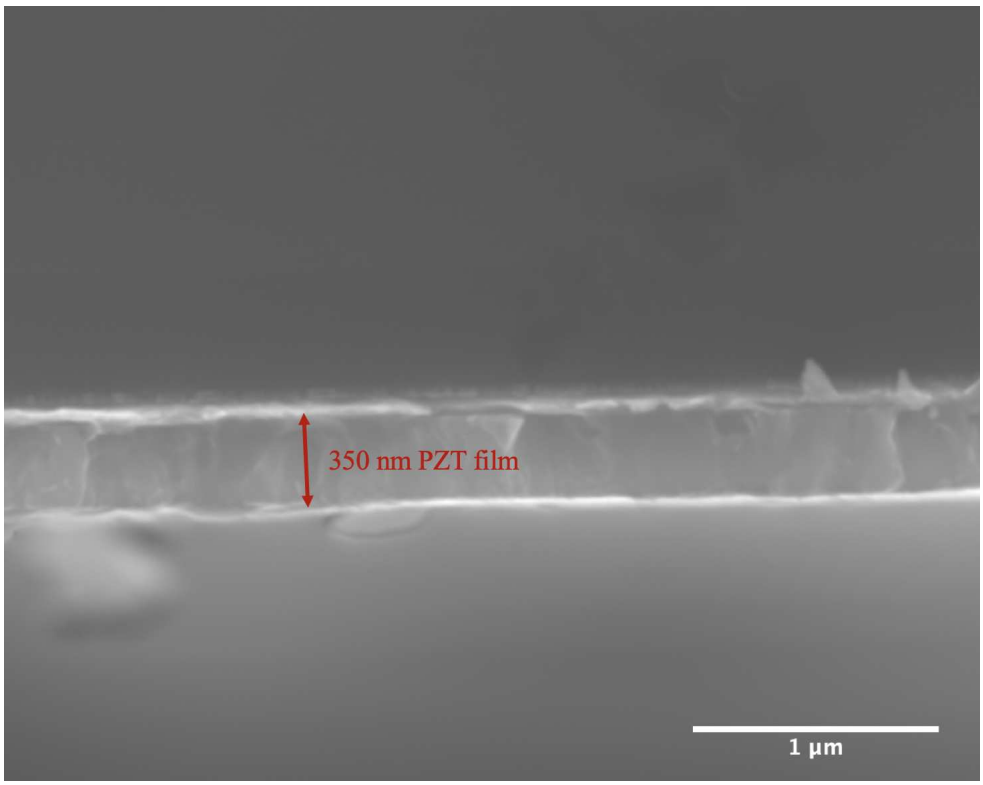

Figure 3.5: FESEM Image of Cross Section of Three Layer PZT Film.

for all films that were characterized with XRD, but did not show a significant degradation to the ferroelectric properties of the material. This result verifies that perovskite PZT films were created through a CSD process.

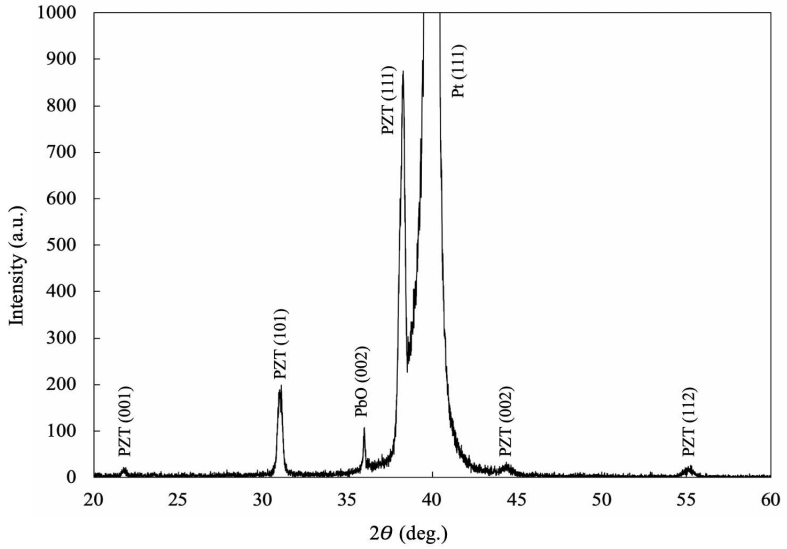

Figure 3.6: X-Ray Diffraction Pattern for PZT Thin Films on Platinized Silicon Substrates.

To account for lead volatility during crystallization, a study was performed to determine the correct amount of excess Pb to add to the solutions. Solutions were fabricated with 10%, 15%, 20% and 30% Pb excess and examined using XRD. The patterns are shown in Figure 3.7 and the broad peaks around 29° and 32° indicate the presence of a fine grained pyrochlore phase at higher Pb excess amounts. These pyrochlore peaks decrease with the reduction in Pb excess, and disappear with 10% Pb excess. This indicates that the peaks arise from a lead-rich pyrochlore phase which is diminished by decreasing the amount of excess Pb in the system. From this study, it was determined that films should be fabricated with 10% Pb excess to eliminate the possibility of a pyrochlore phase that could impact ferroelectric properties.

The microstructure was imaged through an FESEM, and grain size was calculated to be 160±13nm for a three layer PZT film sample on platinized silicon. Figure 3.8 (a) shows the

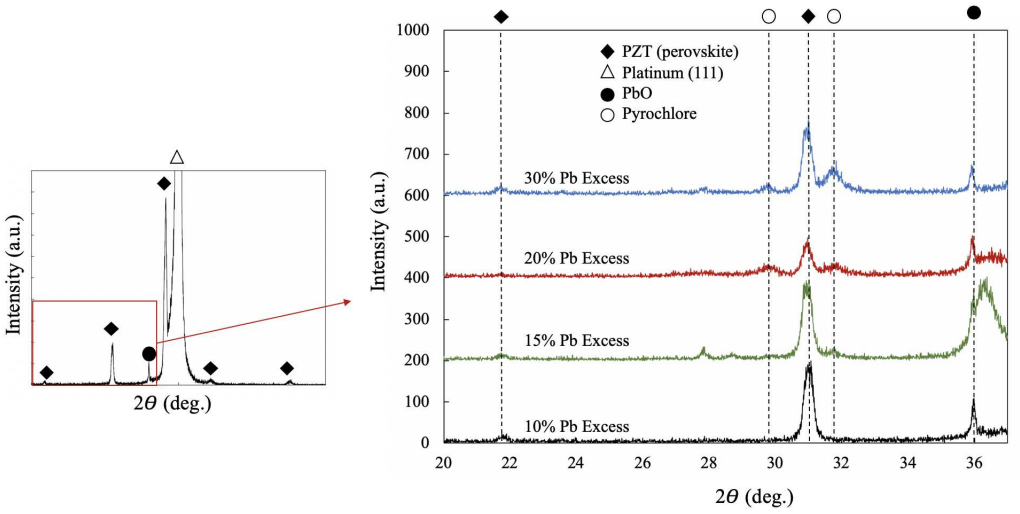

Figure 3.7: X-Ray Diffraction Patterns for PZT Films Processed with Varying Amounts of Pb Excess.

microstructure, consisting of larger grains surrounded by many smaller grains. Figure 3.8 (b) more clearly shows the presence of pinholes within the top layer. The effect of these pin holes were mitigated by the addition of multiple layers, which would reduce the possibility of a single pin holed extending from the top of the film to the bottom electrode, which would cause shorts in the film.

3.4.4 Ferroelectric Measurements

The first set of ferroelectric measurements in this study were made on PZT films that were 350 - 400nm in thickness deposited on platinized silicon substrates with Cu electrodes deposited on top. These samples showed ferroelectric hysteresis when an electric field was applied in either direction, but the loops were asymmetric and had a gap between the start and end of the loop, as shown in Figure 3.9. The asymmetry between the top and bottom of the loop can be attributed to the difference in switching characteristics at the PZT/Pt interface compared to the PZT/Cu interface. Each interface between the PZT and the electrode forms a Schottky (rectifying) barrier. Platinum has a much higher potential barrier with PZT than copper, which leads to the asymmetric shape of the hysteresis loop.

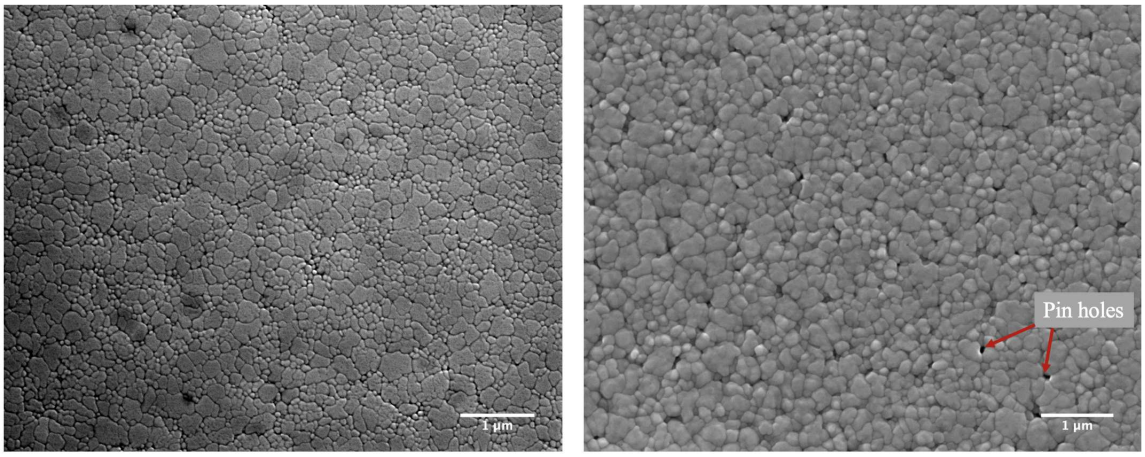

Figure 3.8: FESEM Images of PZT Film Microstructure: (a) Shows Grain Distribution (b) Shows Presence of Pinholes.

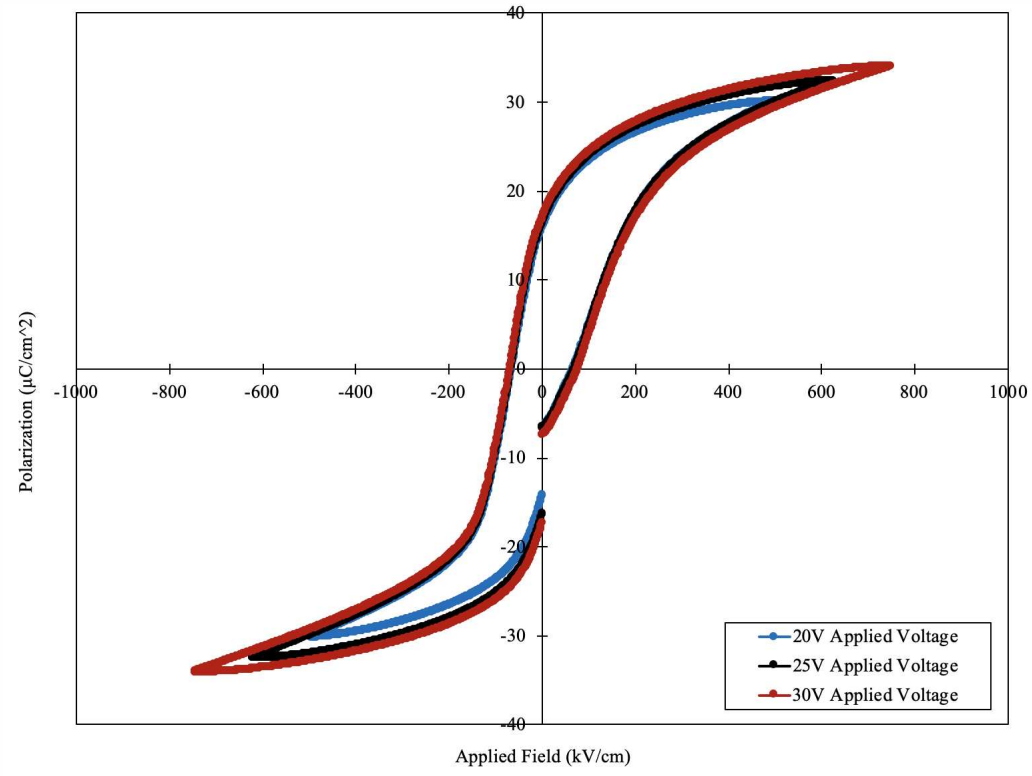

Figure 3.9: Ferroelectric Hysteresis Loops for PZT Film with Cu Top Electrodes.

The next set of hysteresis measurements were made on similar PZT films deposited on platinized silicon substrates, but with Au electrodes deposited on top, shown in Figure 3.10. These loops showed much less asymmetry than the loops obtained with Cu top electrodes, as well as a much smaller gap between the beginning and end of the loop. This also affirms that the asymmetry was due to the difference in potential barriers at each electrode interface, as Au has a much closer work function to Pt than Cu does ($\phi_{Pt} = 5.93$eV, $\phi_{Au} = 5.47$eV, $\phi_{Cu} = 5.10$eV [85]). A platinum top electrode that matched the bottom electrode would eliminate the asymmetry, however sputtering of platinum was not available during the time period of this study.

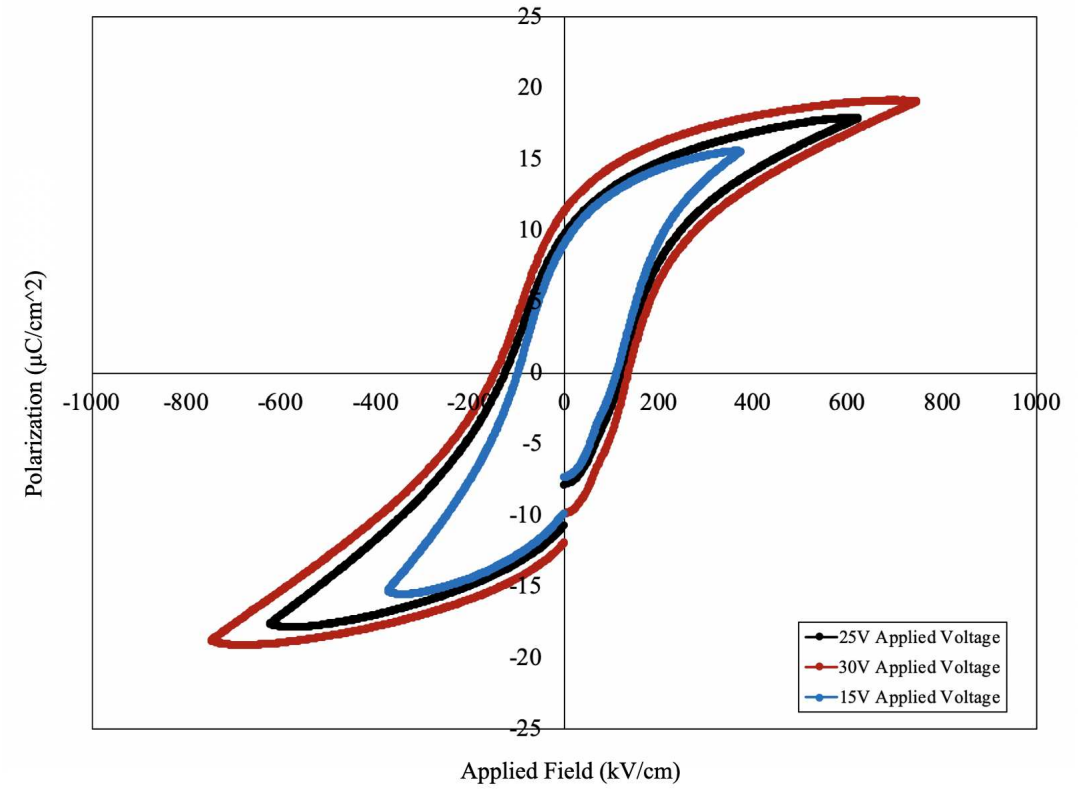

Figure 3.10: Ferroelectric Hysteresis Loops for PZT Film with Au Top Electrodes.

CHAPTER 4

LANTHANUM NICKELATE THIN FILMS

4.1 Motivation and Constraints

Once quality ferroelectric PZT films were obtained on planar substrates, the next step was to develop quality LNO films to use as a bottom electrode for the non-planar silicon substrates. This required first processing LNO films on flat substrates and characterizing them. In this study, "quality" LNO films possess the following qualities: continuity, uniform thickness, and conductive characteristics. Continuity is important so that the PZT does not contact the silicon substrate at all, which would lead to Pb diffusion into the silicon. Continuity and uniform thickness also ensure that the properties are consistent throughout the film area. Finally, the films must display conductivity in order to be used as a bottom electrode.

4.2 Preparation of LNO Thin Films

4.2.1 Substrate Preparation

The substrates used for preparation of the LNO films were high temperature Eagle XG glass from Corning and flat silicon wafers, to more closely match the silicon wedge that is used for the non-planar deposition. Bare silicon oxidizes in air, creating an insulating native oxide layer on the surface that must be removed. To remove this oxide layer, a standard 20:1 deionized (DI) water:hydrogen fluoride (HF) buffered oxide etch was used. The substrate was submerged for 15 seconds in the etchant, removed and submerged in DI water for 1 minute. The CSD films were deposited shortly after the etch step to avoid growth of a new oxide layer.

4.2.2 Thin Film Preparation of $LaNiO_3$ Coated Substrates

4.2.2.1 Solvent Selection

LNO solutions were created through a simple MOD process using two solvents to dissolve the acetate precursors. While much of the literature uses 2-MOE as a solvent in LNO solution chemistry, as mentioned previously, it is a teratogen, mutagen and carcinogen. For this reason, other solvents were tested for the LNO solution chemistry. Originally, DI water and ethanol were chosen as they form an azeotrope and therefore do not evaporate separately. However, when used as solvents for the LNO solution, they did not fully wet the substrate during spin or dip coating, resulting in a film that was not continuous. The next pair of solvents chosen for the LNO solution were acetic acid and methanol. This pairing again did not allow the solution to fully wet the substrate, and also did not evaporate fully during the spin deposition, which led to further issues during the pyrolysis stage. With further research, it was determined that the water/ ethanol and acetic acid/ methanol combinations do not pass Birnie's test for rational solvent selection [56].

2-butoxyethanol was explored, due to its similarities with 2-MOE, the common solvent used in LNO solution creation in literature. While similar to 2-MOE, 2-BOE does not pose the same health hazards. Using Birnie's test, 2-BOE (vapor pressure = 106 Pa and surface tension = 26.14 mN/m) could be paired with DI water to avoid striations [56]. This solution proved to wet the substrate fully, evaporate during deposition, and create films with uniform thicknesses, and therefore was chosen for the processing of the LNO thin films for the rest of this work.

4.2.2.2 Methods

Solutions were made at 0.08 moles/liter and 0.35 moles/ liter for dip coating and spin coating respectively. Lanthanum (III) acetate hydrate (>99.99%, Sigma Aldrich) and nickel (II) acetate tetrahydrate (98%, Sigma Aldrich) were added in stoichiometric amounts to a glass vial. The solvent selection process is discussed in section 4.2.2.1, but the final solvents

chosen for this MOD approach were 2-butoxyethanol (2-BOE) and DI water. 2-BOE was added to dissolve the precursors, and DI water was added to dilute the solution to the final molarity in a ratio of 60% 2-BOE 40% DI water. The solution was mixed until the precursors were dissolved, resulting in a transparent green solution. The solution was then deposited either by spin coating onto a substrate at 4000 rpm for 30 seconds or dip coated at a rate of 5mm/sec onto a bare silicon wafer. Following deposition, a pyrolysis step was performed on a hot plate for 1 minute at 400°C. Deposition and pyrolysis were each performed twice before the film was crystallized at 700°C for 20 minutes.

4.3 Characterization Techniques

The same techniques were used to characterize the crystallinity and microstructure of the films as detailed in Chapter 3. To determine the conductivity of the LNO films, four point probe measurements were taken using a EQ-JX2008-LD Resistivity Tester from MTI Corporation. The probe reports a voltage measured when a certain current is passed through the material. From this voltage, a sheet resistance can be calculated, and multiplied by the thickness of the film to get a resistivity measurement.

4.4 Results and Discussion

4.4.1 Visual Film Quality

The solvent selection process for the LNO films was based solely on the visual film quality, i.e. the full uniform coverage of the substrate with no cracks. As shown in Figure 4.1 (a), the original solvent pairing of water and ethanol barely wet the glass substrate at all during a spin process. A full coverage LNO film is necessary, as the PZT should not contact the underlying substrate at any point. The next solvent pairing used was methanol and acetic acid, as shown in Figure 4.1 (b). This pairing allowed the film to cover the glass substrate more fully, but still displayed some wetting issues around the edges of the film. This film also presented a dark color after crystallization, which indicates a potentially conductive film. This solvent pairing was not chosen however, as it did not fully evaporate during deposition,

which led to thickness variations throughout the film and could cause potential issues on a non-planar substrate, such as pooling in the three-dimensional features. The final pairing of solvents tested was 2-butoxyethanol and DI water, the film of which is shown in Figure 4.1 (c). For this film, a dip coating method was used to deposit the solution onto a silicon substrate, to more closely resemble the wedge material. As shown, this film fully wet the substrate and showed a relatively even thickness throughout the film. This solvent pairing was shown as it reliably provided full even coverage of the substrates.

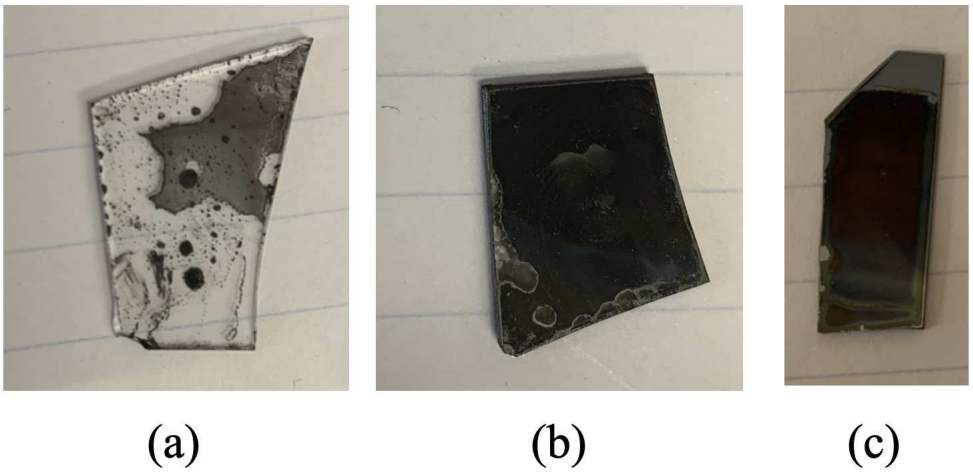

Figure 4.1: LNO Films Created with Different Solvents: (a) Water and Ethanol (b) Acetic Acid and Methanol (c) 2-butoxyethanol and Water.

4.4.2 Crystallinity and Microstructure

The grain structure and crystallinity of the LNO films were determined through FESEM imaging. It is important to examine the grain structure and presence of pin holes to determine if the film provides full coverage. As shown in Figure 4.2, the film has a fine-grained structure with grains on the order of 20nm. The microstructure also displayed the presence of many pin holes (dark spots). This result is initially concerning, as the LNO films must provide full coverage as a bottom electrode for the ferroelectric PZT films. However, multiple layers of LNO film would combat the possibility of the pin holes extending through the thickness of the film.

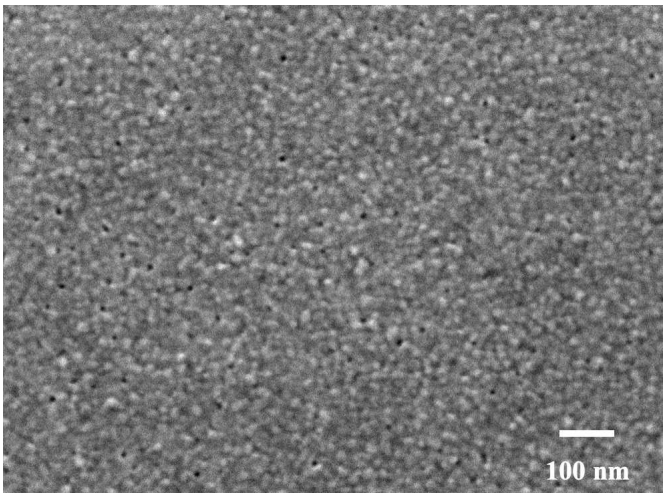

Figure 4.2: FESEM Image of LNO Grain Structure.

4.4.3 Conductivity Measurements

Conductivity of the LNO films was measured with a four point probe. These measurements showed a very low resistivity of the films, between 0.02 - 0.06 mΩ·cm. This low resistivity means that the films are sufficiently conductive to perform as a bottom electrode for the PZT films. The resistivity did not fluctuate much when the film was measured in multiple locations, staying within the range indicated before. This is encouraging, as it means the film has consistent properties throughout.

CHAPTER 5

DEPOSITION ON NON-PLANAR SUBSTRATES

5.1 Motivation and Constraints

CSD techniques have not been widely researched for deposition on substrates with three-dimensional features or non-planar surfaces, so this study looks to develop a reliable method of depositing PZT films onto these types of substrates. Once it was determined that quality PZT and LNO films could be created through chemical solution deposition methods, a method was developed to coat non-planar substrates. Collaborators at ISU requested PZT films to be deposited on silicon wedge substrates for an in-situ dielectric breakdown TEM setup in which they would observe the dielectric breakdown of PZT (and other dielectric materials) within a single grain at the tip of the wedge. The requirements for their testing were a continuous PZT grain on the tip of the wedge and a thin enough film at the tip to be electron transparent. From a processing standpoint, this means developing a continuous film that evenly coats the wedge at the tip. Constraints that were considered in this portion of the work included the dimensions of the wedge and the wedge material. For this specific application, alterations were made to the substrate, such as etching and thinning the wedge to comply with the collaborator requirements. However, when applying these methods to other types of non-planar substrates, these constraints may not be the same, and alterations may not need to be made to the substrate.

5.2 Sample Preparation

5.2.1 Substrate Preparation

The non-planar substrate used was a silicon wedge that is typically used for nanoindentation obtained from Bruker. The wedge is shown in Figure 5.1. These wedges are used by collaborators at ISU to investigate *in-situ* dielectric breakdown in a TEM. The purpose of this study is to develop a method to evenly coat the entire wedge with a chemical solution

deposited film. The same buffered oxide etch used on the flat silicon substrates was used for the silicon wedges as well to remove the native oxide layer.

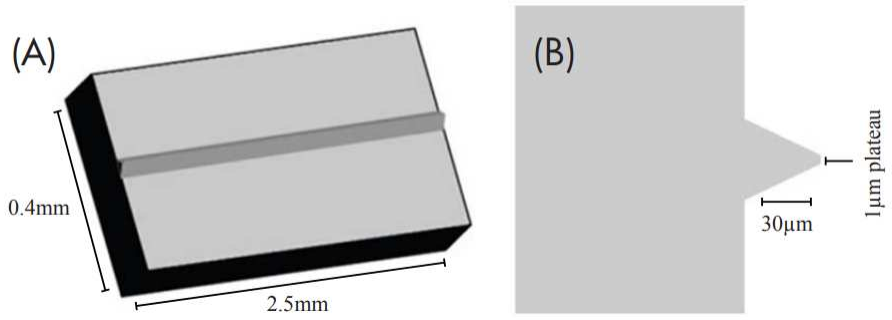

Figure 5.1: Schematic of Silicon Wedge Substrate: (A) Top Down View, (B) Cross Sectional View.

For the TEM experiment, it was necessary for the film to be thin enough at the tip of the wedge to be electron transparent. After consultation with collaborators, it was determined that no matter how thin the deposited film was, the shape of the substrate did not allow for an electron transparent film at the tip. The schematic in Figure 5.2 shows the explanation and requirement for this application.

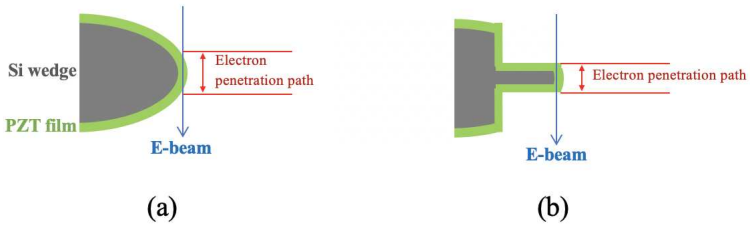

Figure 5.2: Schematic of Requirements for Substrate Size: (a) As-Purchased Wedge with Film (b) Ideal Wedge Shape with Film. Courtesy of Xiaoli Tan and Xinchun Tian, ISU.

A focused ion beam (FIB) technique was used with help from David Dierks at Colorado School of Mines to thin down the sides of the wedge and create a plateau on the order of 100-200nm along $\sim$50μm sections of the wedge. A side view of the altered wedge is shown

in Figure 5.3. The shape of the thinned substrate corresponds to the required shape shown in Figure 5.2 (b).

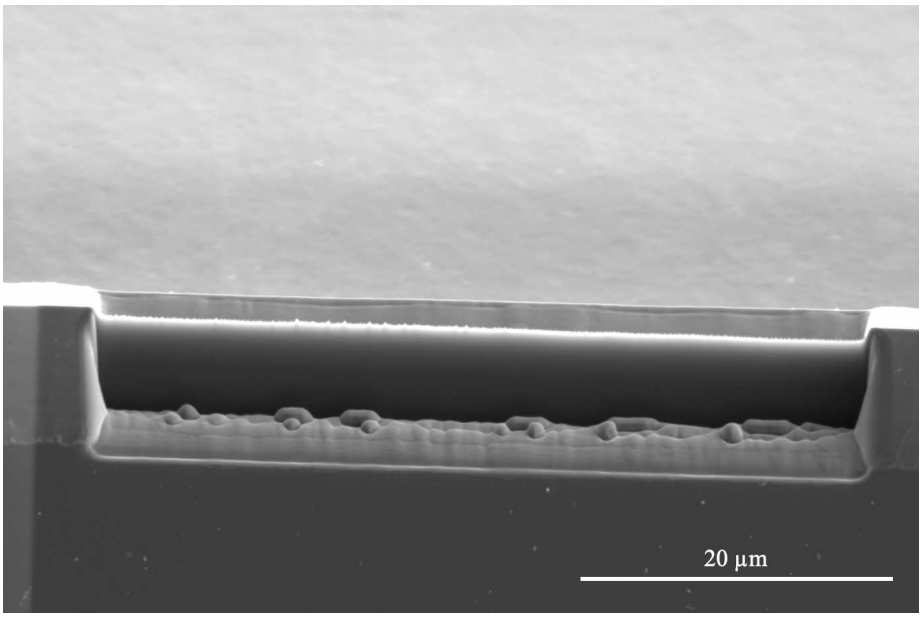

Figure 5.3: Side View of Thinned Wedge Sample, Courtesy of David Dierks (CSM).

5.2.2 Deposition of LNO and PZT Thin Films onto a Silicon Wedge

A dip coating method was used to deposit films of LNO and PZT onto the wedge substrate from solution. The LNO solution used was 0.08M and the PZT solution used was 0.1M. To deposit each layer, the substrate was lowered into the appropriate solution and removed at a steady rate. Initially this dipping was done by hand at a rate that was calculated to be approximately 5mm/sec. For samples that were to be tested for thickness and uniformity, a Ni-Lo X1 Dip Coater from Nilo Scientific was used. This dip coater only allowed a removal rate of around 1mm/sec, and therefore deposited much thicker films. It was determined that for the wedge substrates, the necessary thickness was best obtained through dip coating by hand, as the molarity of the solutions was already very low, and any reduction of this would potentially lead to island formation in the film upon crystallization. Between each layer, a 1 minute pyrolysis step was performed on at hot plate at 400°C. Two layers of LNO were deposited and then crystallized at 700°C for 20 minutes. After the LNO was crystallized, two

layers of PZT were deposited, with pyrolysis steps between each, followed by a crystallization step at 700°C for 10 minutes. Sister samples were created on flat substrates with the same deposition and heating parameters to allow for characterization.

5.2.2.1 Nylon Wire to Reduce Surface Tension Effects

Due to the thin nature of the silicon wedge substrates, it was determined that surface tension effects were leading to a buildup of solution towards the bottom of the substrates, causing much thicker films than were measured on the flat sister substrates. A method was developed to combat these surface tension effects by attaching a 0.2mm nylon wire behind the substrate while dipping. The idea behind this was to allow the solution to continue to drip down the wire instead of building up on the end of the substrate. By providing an alternate route for the solution to move, it should help thin the film on the wedges. The nylon wire setup is shown in Figure 5.4. The films were dip coated with the same parameters as described in section 5.2.2. This method was used on both the as-purchased substrates and the FIB-thinned substrates.

5.2.2.2 PZT Nanoparticles

Along with thin films, PZT nanoparticles were synthesized from the IMO solutions, intended to be dispersed onto the tip of the non-planar wedge substrate. Patent No. 5,908,802 was used as a basis for this process [86]. To achieve this, a typical 0.35M PZT IMO solution with 20% Pb excess was created. Oxalic acid (>99%, Sigma Aldrich) was dissolved in methanol at 50°C to achieve a molarity of ∼6 moles/liter and added to the PZT solution in a ratio of 3 moles oxalic acid to 1 mole of cations. This quickly caused a precipitation reaction. The precipitate was separated from the liquid through drying at 90°C. Once all the solvents were dried, the precipitate was slowly (5°C/ min) heated to a temperature of 350°C to remove the rest of the organic material. Upon reaching this temperature, the white precipitate began to turn brown, and once fully brown the powder was removed from the heat. The powder was then calcined at 600°C for 3 hours to achieve a phase pure perovskite

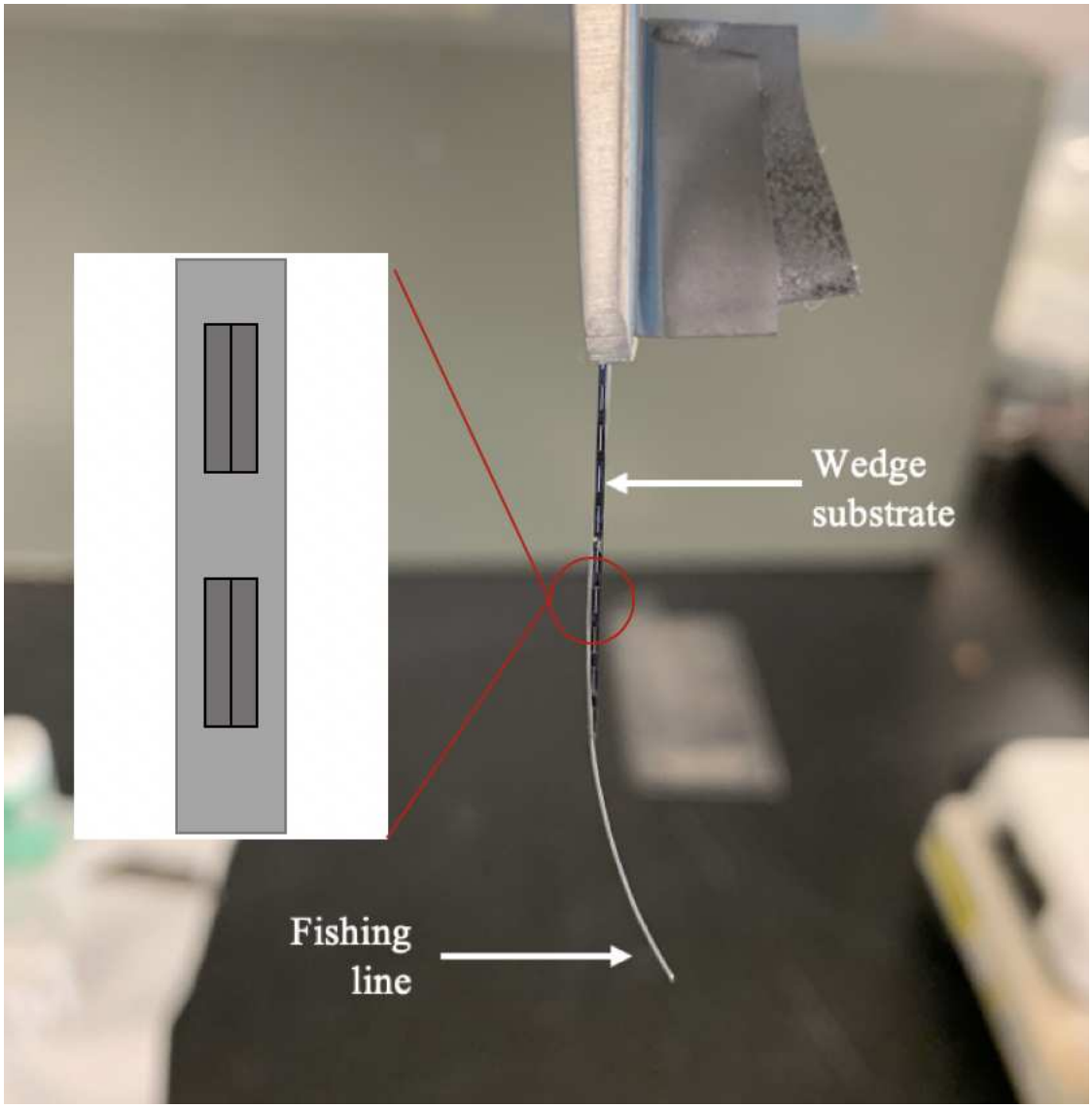

Figure 5.4: Setup for Dip Coating with Nylon Wire Attachment, With Schematic of Two Wedges on Substrate (inset).

powder.

5.3 Characterization Techniques

Much of the characterization of the films deposited on the wedge substrates was performed by collaborators at ISU using SEM and TEM imaging techniques. The characterization performed mainly focused on the viability of the films for their dielectric breakdown measurements, however the images obtained were still useful to characterize the deposition of the films on the non-planar substrates. The PZT nanoparticles were characterized by XRD and FESEM to verify perovskite structure and determine particle size.

5.4 Results and Discussion

5.4.1 Dip Coated Films on Original Wedge Substrate

The films that were deposited on the as-purchased silicon substrates were sent to collaborators at ISU, where they were imaged using both SEM and TEM techniques. Figure 5.5 shows the film deposited along the surface of the wedge. While some cracks can be seen on the surrounding substrate, no cracks were visible on the wedge itself. The film does not look evenly coated along the length of the wedge, however some topography can be seen that indicated the film does follow the wedge-like shape of the substrate. The thickness of sister films was measured to be on the order of 50 nm, however due to surface tension effects, the thickness of the film on the wedge proved to be much higher than the films deposited on the flat substrates.

The film was too thick at the tip for ISU collaborators to be able to observe dielectric breakdown, as this film was deposited on the a wedge that had not been thinned via FIB. TEM images were also obtained at ISU, shown in Figure 5.6. The PZT film itself, rather than the substrate, was instead thinned via FIB, and showed a crystalline nature, which validates that a crystalline PZT film was successfully deposited on the wedge substrate. The total thickness of the coating (two layers of LNO with two layers of PZT on top) was about 100nm. The dark spots that show up in the TEM images are Ga contamination from the

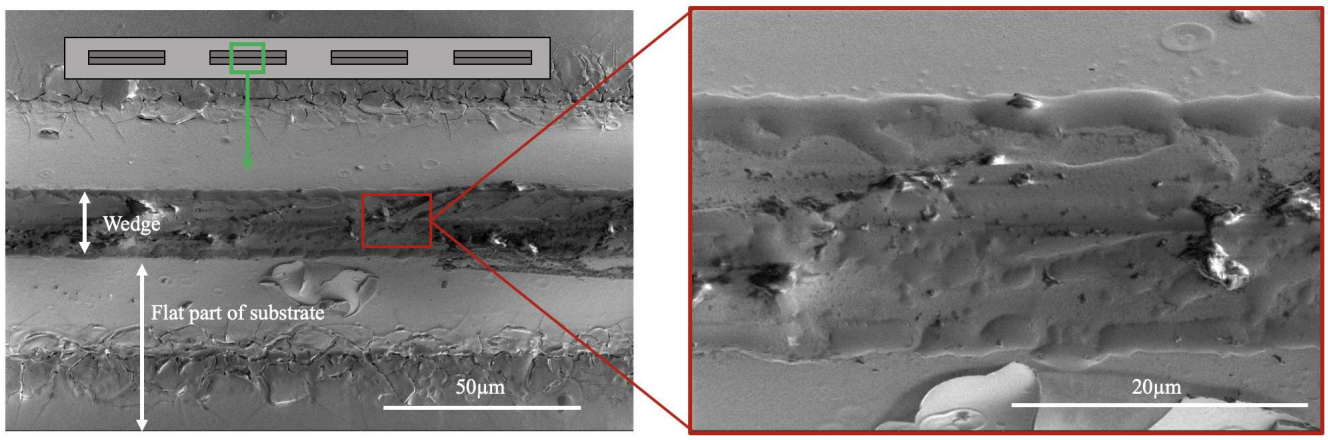

Figure 5.5: SEM Image of PZT Film on the Wedge Substrate, 2.00kV Accelerating Voltage, Ames Lab Helios, Courtesy of Xiaoli Tan and Xinchun Tian, ISU.

FIB which was used to thin the PZT to an electron transparent thickness. This method of thinning the film after its deposition is not ideal, due to the Ga contamination that could alter the dielectric breakdown of the PZT.

5.4.2 Dip Coated Films using Nylon Wire

Silicon wedges coated using the nylon wire method from section 5.2.2.1 were weighed after each layer and pyrolysis step to be compared to the wedges dip coated without wire. No change was seen in the difference in weight from the two different methods using a scale that accurately displayed to four decimal points. Collaborators at ISU received the samples, and were able to image them. The films were thin at the wedge tip, but quickly became too thick down the wedge to be used for the *in-situ* TEM experiment. This reaffirmed the assumption that the wedge itself is not thin enough at the tip to allow for an electron transparent path for the experiment, and the wedge must be thinned.

5.4.3 Dip Coated Films on Wedges Modified by FIB

The wedge samples that were thinned with FIB were coated in two layers of LNO followed by two layers of PZT using the nylon wire technique described in section 5.2.2.1. This was

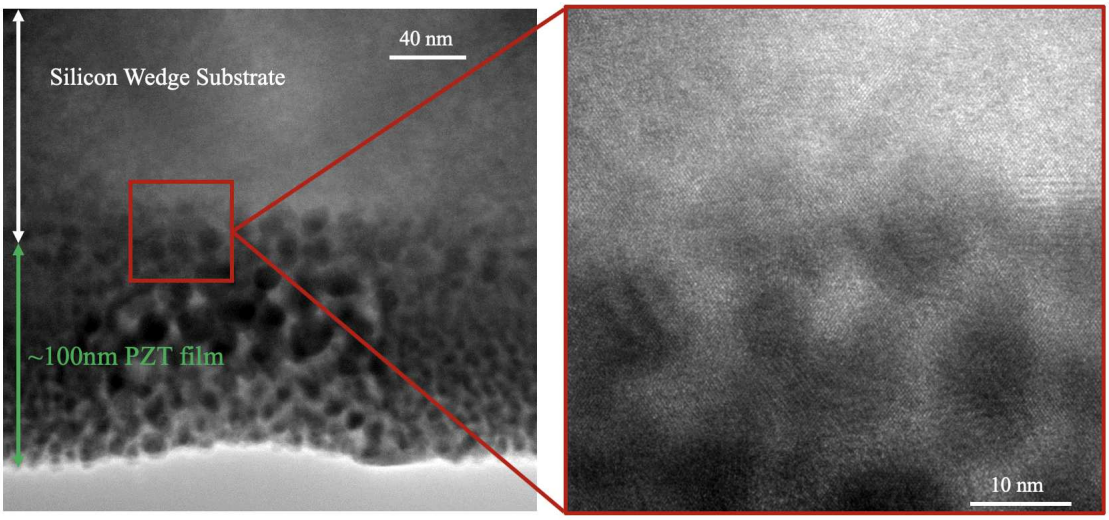

Figure 5.6: TEM Images of PZT Film on Wedge, Courtesy of Xiaoli Tan and Xinchun Tian, ISU.

essential to the deposition on the thin wedges, as pooling of the solution is very likely to occur in the newly created divots in the sample.

5.4.4 PZT Nanoparticles

Nanoparticles of PZT were synthesized and characterized through various techniques.

5.4.4.1 Crystallinity and Particle Size of Powders

The perovskite structure of the PZT powders was verified with XRD. While a clear perovskite structure was present, some pyrochlore peaks showed up around 29° and 32°. The absence of a low angle (∼12°) peak pointed to a lead-rich fluorite phase, and not the lead-deficient, non-ferroelectric pyrochlore phase that would degrade ferroelectric properties. This makes sense, as it is easy for the system to lose lead due to its volatility and transform from a lead-rich fluorite phase into the perovskite phase. These peaks could be reduced by lowering the lead excess to 10% rather than 20% to hopefully impede the crystallization of a lead-rich phase.

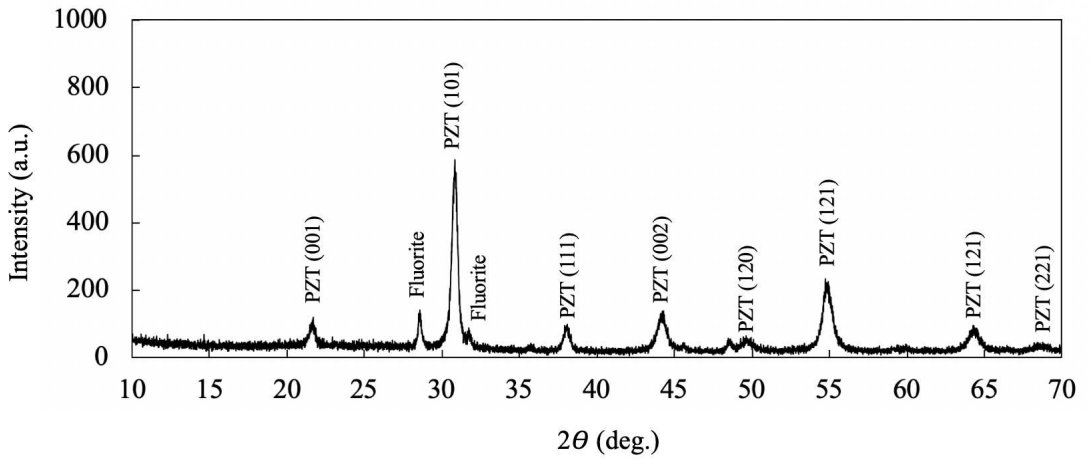

Figure 5.7: X-Ray Diffraction Pattern of PZT Nanoparticles.

The PZT particles were imaged with FESEM to determine particle size. As shown in Figure 5.8, the particles are on the order of 60nm in diameter with larger particles approaching 100nm and smaller ones around 40nm. This information is enough to conclude that nanoparticles were created, and their sizes are smaller than the plateau at the tip of the silicon wedge (1μm). This is imperative for the nanoparticle dispersion and deposition process, as the goal is to have a single nanoparticle sitting on the plateau. At these particle sizes, it is very likely that particles will be able to sit on the wedge plateau after dispersion.

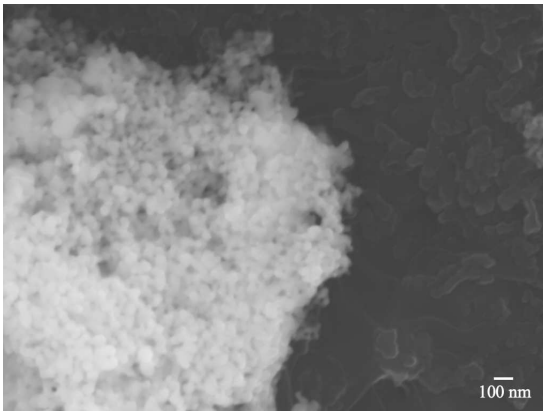

Figure 5.8: FESEM Image of PZT Nanoparticles.

CHAPTER 6
CONCLUSIONS

6.1 Conclusions

1. Ferroelectric perovskite PZT films were made through the IMO chemical solution deposition technique. The films were characterized through XRD, SEM and hysteresis measurements. The films displayed a perovskite structure with small amounts of PbO present. The PbO did not impact the ferroelectric nature of the films. A lead excess in solution of 10% was determined to eliminate a lead-rich pyrochlore phase that showed up in films with higher Pb excess amounts. The microstructure was imaged, and determined to be columnar from the substrate, with a grain size of 160 nm. The thicknesses of the films were shown to vary linearly with the number of layers, and a single layer of spin coated PZT was shown to be 115 nm in thickness. The films displayed ferroelectric hysteresis in their P-E loop behavior. Copper electrodes were initially used and resulted in asymmetric hysteresis loops due to the difference in potential barrier height between the Cu/ PZT and Pt/ PZT interface. Gold electrodes had a similar barrier height when interfaced with PZT to the platinum/ PZT interface and showed more symmetric hysteresis loops. All these characteristics lead to the conclusion that "quality" PZT films were made in the context of this work.

2. Conductive LNO films were created through a MOD solution deposition method. Pin holes were visible in the FESEM images, but did not appear to affect the conductivity of the film throughout its area. To adjust for pin holes, multiple layers of LNO were deposited. Multiple solvents were tested for the LNO solutions, with a mixture of 2-BOE and DI water proving to produce films that fully covered the substrate and produced a uniform thickness. Each dip coated layer of LNO from a 0.08M solution was found to be around 100 nm in thickness. Low resistivity between 0.02 - 0.06 mΩ·cm

was measured for the LNO films, confirming the viability of these films as a bottom electrode for PZT.

3. LNO and PZT thin films were successfully deposited onto the non-planar wedge substrate. Although the thickness of the films originally dip coated was much too high for the wedge application, the FESEM images clearly show a film that follows the contour of the wedge substrate. This method of dip coating could be applied to other non-planar substrates, with some alterations depending on the size and shape of the substrate.

4. A dip coating method was developed to reduce the thickness of the films by reducing surface tension effects that caused the solution to build up at the bottom of the substrate. This method, which included attaching 0.2mm nylon wire to the dip coating setup, did not prove to reduce the weight of the film deposited. However, it did provide a thinner film at the tip of the silicon wedge. This method could be applied to other thin substrates which may experience similar surface tension effects. This was still too thick for the targeted in-situ TEM study, so the wedges had to be thinned down by FIB to accommodate.

5. Perovskite PZT nanoparticles were created, with some lead-rich pyrochlore phase present. These nanoparticles are intended to be dispersed on the tip of the silicon wedge through a method successfully done by collaborators at ISU, and provide yet another way to deposit nanometers of PZT material onto a non-planar substrate.

6. Ongoing work with the samples created in this thesis is occurring at Iowa State University. The TEM study is being performed by collaborators Dr. Xiaoli Tan and Dr. Xinchun Tian. They will carry on the dielectric breakdown study on the films and nanoparticles created in this work.

REFERENCES CITED

[1] X. Tian, C. Cook, W. Hong, T. Ma, G. L. Brennecka, and X. Tan. In Situ TEM Study of the Amorphous-to-Crystalline Transition during Dielectric Breakdown in TiO 2 Film. *ACS Applied Materials & Interfaces*, 2019.

[2] B. Jaffe, W. R. Cook, and H. Jaffe. *Piezoelectric Ceramics*. Academic Press, 1971.

[3] N. Izyumskaya, Y. I. Alivov, S. J. Cho, H. Morkoç, H. Lee, and Y. S. Kang. Processing, structure, properties, and applications of PZT thin films. *Critical Reviews in Solid State and Materials Sciences*, 32(3-4):111–202, 2007.

[4] R. Ramesh, S. Aggarwal, and O. Auciello. Science and technology of ferroelectric films and heterostruc-tures for non-volatile ferroelectric memories. *Materials Science and Engineering*, 32:191–236, 2000.

[5] P. Muralt. Ferroelectric thin films for micro-sensors and actuators: a review Related content. *Journal of Micromechanics and Microengineering*, 10:136–146, 2000.

[6] J. F. Tressler, S. Alkoy, and R. E. Newnham. Piezoelectric Sensors and Sensor Materials. *Journal of Electroceramics*, 2(4):257–272, 1998.

[7] S. S. N. Bharadwaja, M. Olszta, S. Trolier-McKinstry, X. Li, T. S. Mayer, and F. Roozeboom. Fabrication of high aspect ratio ferroelectric microtubes by vacuum infiltration using macroporous silicon templates. *Journal of the American Ceramic Society*, 89(9): 2695–2701, 2006.

[8] T. G. Cooney and L. F. Francis. Processing of sol-gel derived PZT coatings on non-planar substrates. *J. Micromech. Microeng*, 6:291–300, 1996.

[9] E. A. Mikalsen and D. A. Payne. Additive deposition and patterning of ferroelectric materials on non-planar surfaces by chemical-solution methods. *IEEE International Symposium on Applications of Ferroelectrics*, 1:417–420, 2000.

[10] J. D. Mackenzie. Applications of the sol-gel process. *Journal of Non-Crystalline Solids*, 100(1-3):162–168, mar 1988.

[11] D. E. Bornside, C. W. Macosko, and L. E. Scriven. On the Modeling of Spin Coating. *Journal of Imaging Technology*, 13:122–130, 1987.

[12] R. Ramesh, S. Aggarwal, and O. Auciello. Science and technology of ferroelectric films and heterostruc-tures for non-volatile ferroelectric memories. *Materials Science and Engineering*, 32:191–236, 2001.

[13] B. Noheda, D. E. Cox, G. Shirane, J. A. Gonzalo, L. E. Cross, and S. E. Park. A monoclinic ferroelectric phase in the Pb(Zr1-xTix)O3 solid solution. *Appl. Phys. Lett*, 74:2059, 1999.

[14] W. D. Kingery, H. K. Bowen, and D. R. Uhlmann. *Introduction to Ceramics*. John Wiley & Sons, Inc., 2nd editio edition, 1960.

[15] J. F. Ihlefeld, D. T. Harris, R. Keech, J. L. Jones, J. P. Maria, and S. Trolier-McKinstry. Scaling Effects in Perovskite Ferroelectrics: Fundamental Limits and Process-Structure-Property Relations. *Journal of the American Ceramic Society*, 99(8):2537–2557, 2016.

[16] T. M. Shaw, S. Trolier-Mckinstry, and P. C. Mcintyre. The Properties of Ferroelectric Thin Films at Small Dimensions. *Annual Review of Materials Science*, 30:263–298, 2000.

[17] G. A. Rossetti, L. E. Cross, and K. Kushida. Stress induced shift of the Curie point in epitaxial PbTiO3 thin films. *Appl. Phys. Lett*, 59:2524, 1991.

[18] N. A. Pertsev, A. G. Zembilgotov, S. Hoffmann, R. Waser, and A. K. Tagantsev. Ferroelectric thin films grown on tensile substrates: Renormalization of the Curie-Weiss law and apparent absence of ferroelectricity. *Journal of Applied Physics*, 85:1698, 1999.

[19] M. Algueró, M. L. Calzada, M. J. Martın, and L. Pardo. A layer of reduced switchable polarisation in (Pb,La)TiO3 films leading to a thickness dependence of the ferroelectric parameters. *Journal of Physics and Chemistry of Solids*, 63(3):471–481, mar 2002.

[20] K. Amanuma, T. Mori, T. Hase, T. Sakuma, A. Ochi, and Y. Miyasaka. Ferroelectric Properties of Sol-Gel Derived Pb(Zr, Ti)O3 Thin Films. *Japanese Journal of Applied Physics To*, 32:4150, 1993.

[21] P. K. Larsen, G. J. M. Dormans, D. J. Taylor, and P. J. Van Veldhoven. Ferroelectric properties and fatigue of PbZr0.51Ti0.49O3 thin films of varying thickness: Blocking layer model. *Journal of Applied Physics*, 76:2405, 1994.

[22] K. b. Blodgett Vol and E. K. Rideal. Films Built by Depositing Successive Monomolecular Layers on a Solid Surface. *Journal of the American Ceramic Society*, 109:301, 1935.

[23] H. Dislich. New routes to multicomponent oxide glasses. *Angewandte Chemie International Edition*, 6:363, 1971.

[24] R. Roy. Aids in Hydrothermal Experimentation: II, Methods of Making Mixtures for Both "Dry" and "Wet" Phase Equilibrium Studies. *Journal of the American Ceramic Society*, 75(11):2931–2932, 1956.

[25] R. Roy. Gel Route to Homogeneous Glass Preparation. *Journal of the American Ceramic Society*, 52(6):344–344, 1969.

[26] R. Roy. Ceramics by the Solution-Sol-Gel Route. *Science*, 238(4834):1664–1669, 1965.

[27] G. J. McCarthy, R. Roy, and J. M. McKay. Preliminary Study of Low-Temperature "Glass" Fabrication from Noncrystalline Silicas. *Journal of the American Ceramic Society*, 54(12):637–638, 1971.

[28] H. Dislich. Sol-gel: Science, processes and products. *Journal of Non-Crystalline Solids*, 80(1-3):115–121, mar 1986.

[29] C.J. Brinker, K.D. Keefer, D.W. Schaefer, R.A. Assink, B.D. Kay, and C.S. Ashley. Sol-gel transition in simple silicates II. *Journal of Non-Crystalline Solids*, 63(1-2):45–59, feb 1984.

[30] K. D. Budd, S. Dey, and D. A. Payne. Sol-Gel Processing of PbTiO//3, PbZrO//3, PZT, and PLZT Thin Films. *British Ceramic Society Proceedings*, pages 107–121, 1985.

[31] J. D. Mackenzie. Glasses from melts and glasses from gels, a comparison. *Journal of Non-Crystalline Solids*, 48(1):1–10, mar 1982.

[32] G. Yi, Z. Wu, and M. Sayer. Preparation of Pb(Zr,Ti)O 3 thin films by sol gel processing: Electrical, optical, and electro-optic properties. *Journal of Applied Physics*, 64:2717, 1988.

[33] R. A. Assink and R. W. Schwartz. Proton and carbon-13 NMR investigations of lead zirconate titanate (Pb(Zr,Ti)O3) thin-film precursor solutions. *Chem. Mater*, 5:511–517, 1993.

[34] J. Fukushima, K. Kodaira, and T. Matsushita. Preparation of ferroelectric PZT films by thermal decomposition of organometallic compounds. *Journal of Materials Science*, 19:595–598, 1984.

[35] K. Sumi, H. Qiu, M. Shimada, S. Sakai, S. Yazaki, M. Murai, S. Moriya, Y. Miyata, and T. Nishiwaki. Dependence of Electrically Induced Strain on Orientation and Composition in Pb(Zr x Ti 1x)O 3 Films. *Japanese Journal of Applied Physics*, 38(8): 4843–4846, 1999.

[36] S. Y. Chen and I. W. Chen. Temperature–Time Texture Transition of Pb(Zr1xTix)O3 Thin Films: I, Role of Pb-rich Intermediate Phases. *Journal of the American Ceramic Society*, 77(9):2332–2336, 1994.

[37] S. Y. Chen and I. M. Chen. Temperature-Time Texture Transition of Pb(Zr,-xTix)03 Thin Films: II, Heat Treatment and Compositional Effects. *Journal of the American Ceramic Society*, 77(9):2337–2344, 1994.

[38] C. D. E. Lakeman, J. Campion, and D. A. Payne. Factors affecting the sol-gel processing of PZT thin layers. *Ceramic Transactions*, 25:413–439, 1992.

[39] I. M. Reaney, D. V. Taylor, and K. G. Brooks. Ferroelectric PZT Thin Films by Sol-Gel Deposition. *Journal of Sol-Gel Science and Technology*, 13:813–820, 1998.

[40] B.A. Tuttle and R.W. Schwartz. Solution Deposition of Ferroelectric Thin Films. *MRS Bulletin*, 21(6):49–54, jun 1996.

[41] M. Kosec, B. Malic, and M. Mandeljc. Chemical solution deposition of PZT thin films for microelectronics. *Materials Science in Semiconductor Processing*, 5(2-3):97–103, apr 2002.

[42] I. M. Reaney, K. Brooks, R. Klissurska, C. Pawlaczyk, and N. Setter. Use of Transmission Electron Microscopy for the Characterization of Rapid Thermally Annealed, Solution-Gel, Lead Zirconate Titanate Films. *Journal of the American Ceramic Society*, 77(5):1209–1216, 1994.

[43] K. G. Brooks, I. M. Reaney, R. Klissurska, Y. Huang, L. Bursill, and N. Setter. Orientation of rapid thermally annealed lead zirconate titanate thin films on (111) Pt substrates. *Journal of Materials Research*, 9(10):2540–2553, 1994.

[44] X. J. Meng, J. G. Cheng, B. Li, S. L. Guo, H. J . Ye, and J. H. Chu. Low-temperature preparation of highly (111) oriented PZT thin films by a modified sol–gel technique. *Journal of Crystal Growth*, 208(1-4):541–545, jan 2000.

[45] R. W. Schwartz. Chemical Solution Deposition of Perovskite Thin Films. *Chemistry of Materials*, 9:2325–2340, 1997.

[46] G. L. Brennecka, J. F. Ihlefeld, J. P. Maria, B. A. Tuttle, and P. G. Clem. Processing technologies for high-permittivity thin films in capacitor applications. *Journal of the American Ceramic Society*, 93(12):3935–3954, 2010.

[47] R. W. Schwartz, J. A. Voigt, and B. A. Tuttle. Comments on the effects of solution precursor characteristics and thermal processing conditions on the crystallization. *Journal of Materials Research*, 12(2):444–456, 1997.

[48] M. D. Carper and P. P. Phulé. Preparation of oriented PbTiO 3 thin films using a spin-on sol-gel process. *Appl. Phys. Lett*, 63:153, 1993.

[49] R. W. Schwartz, R. A. Assink, and T. J. Headley. Spectroscopic and Microstructural Characterization of Solution Chemistry Effects in PZT Thin Film Processing. *Materials Research Society Symposium Proceedings*, 243:245–254, 1992.

[50] G. Yi and M. Sayer. An Acetic Acid/Water Based Sol-Gel PZT Process I: Modification of Zr and Ti Alkoxides with Acetic Acid. *Journal of Sol-Gel Science and Technology*, 6:65–74, 1996.

[51] G. Yi and M. Sayer. An Acetic Acid/Water Based Sol-Gel PZT Process II: Formation of a Water Based Solution. *Journal of Sol-Gel Science and Technology*, 6:75–82, 1996.

[52] C. Sanchez, J. Livage, M. Henry, and F. Babonneau. Chemical modification of alkoxide precursors. *Journal of Non-Crystalline Solids*, 100(1-3):65–76, mar 1988.

[53] S. Barboux-Doeuff and C. Sanchez. Synthesis and characterization of titanium oxide-based gels synthesized from acetate modified titanium butoxide precursors. *Materials Research Bulletin*, 29(1):1–13, jan 1994.

[54] D. Birnie and N. J. Bendzko. 1H and 13C NMR observation of the reaction of acetic acid with titanium isopropoxide. *Materials Chemistry and Physics*, 59(1):26–35, 1999.

[55] T. J. Boyle, D. Dimos, R. W. Schwartz, T. M. Alam, M. B. Sinclaire, and C. D. Buchheit. Aging characteristics of a hybrid sol-gel Pb(Zr,Ti)O3 precursor solution. Journal of Materials Research, 1997. 12(4): p. 1022-1030. *Journal of Materials Research*, 12(4), 1997.

[56] D. Birnie. Rational Solvent Selection Strategies to Combat Striation Formation During Spin Coating of Thin Films. *J Mater Res*, 16(4):1145–1154, 2001.

[57] C. J. Brinker and G. W. Scherer. *Sol-Gel Science The Physics and Chemistry of Sol-Gel Processing*. Academic Press, Boston, 1990.

[58] L. E. Scriven. Physics and Applications of Dip Coating and Spin Coating. *Materials Research Society Symposium: Better Ceramics Through Chemistry III*, 121, 1988.

[59] A. G. Emslie, F. T. Bonner, and L. G. Peck. Flow of a Viscous Liquid on a Rotating Disk. *Journal of Applied Physics*, 29(5):858–862, 1958.

[60] D. Meyerhofer. Characteristics of resist films produced by spinning. *Journal of Applied Physics*, 49:3993, 1978.

[61] C. J. Brinker, A. J. Hurd, G. C. Frye, K. J. Ward, and C. S. Ashley. Sol-gel thin film formation. *Journal of Non-Crystalline Solids*, 121(1-3):294–302, may 1990.

[62] R. P. Spiers, C. V. Subbaraman, and W. L. Wilkinson. Free coating of a Newtonian liquid onto a vertical surface. *Chemical Engineering Science*, 29(2):389–396, feb 1974.

[63] Z. Tio, A. D. Polli, F. F. Lange, and C. G. Levi. Metastability of the Fluorite , Pyrochlore , and Perovskite Structures in. *Journal of the American Ceramic Society*, 81:873–881, 2000.

[64] B. A. Tuttle, T. J. Headley, B. C. Bunker, R. W. Schwartz, T. J. Zender, C. L. Hernandez, D. C. Goodnow, R. J. Tissot, J. Michael, and A. H. Carim. Microstructural evolution of Pb(Zr, Ti)O3 thin films prepared by hybrid metallo-organic decomposition. *Journal of Materials Research*, 7(7):1876–1882, 1992.

[65] C. D. E. Lakeman, Z. Xu, and D. A. Payne. On the evolution of structure and composition in sol-gel-derived lead zirconate titanate thin layers. *Journal of Materials Research*, 10(8):2042–2051, 1995.

[66] C. K. Kwok and S. B. Desu. Pyrochlore to perovskite phase transformation in sol-gel derived lead-zirconate-titanate thin films. *Appl. Phys. Lett*, 60(12):1430, 1992.

[67] K. Nittala, S. Mhin, J. L. Jones, D. S. Robinson, J. F. Ihlefeld, and G. L. Brennecka. In situ x-ray diffraction of solution-derived ferroelectric thin films for quantitative phase and texture evolution measurement. *J. Appl. Phys*, 112:104109, 2012.

[68] J. Harjuoja, S. Väyrynen, M. Putkonen, L. Niinistö, and E. Rauhala. Atomic layer deposition of PbZrO3 thin films. *Applied Surface Science*, 253(12):5228–5232, apr 2007.

[69] T. Watanabe, S. Hoffmann-Eifert, F. Peter, S. Mi, C. Jia, C. S. Hwang, and R. Waser. Liquid injection ALD of Pb (Zr,Ti) Ox thin films by a combination of self-regulating component oxide processes. *Journal of the Electrochemical Society*, 154(12):262–269, 2007.

[70] T. Watanabe, S. Hoffmann-Eifert, C. S. Hwang, and R. Waser. Growth behavior of atomic-layer-deposited Pb(Zr,Ti)Ox thin films on planar substrate and three-dimensional hole structures. *Journal of the Electrochemical Society*, 155(11):715–722, 2008.

[71] J. H. Choi, F. Zhang, Y. C. Perng, and J. P. Chang. Tailoring the composition of lead zirconate titanate by atomic layer deposition. *Citation: Journal of Vacuum Science & Technology B*, 31:12207, 2013.

[72] M. Ichiki, L. Zhang, Z. Yang, T. Ikehara, and R. Maeda. Thin film formation on non-planar surface with use of spray coating fabrication. *Microsystem Technologies*, 10: 360–363, 2004.

[73] S. Y. Ng and A. R. Boccaccini. Lead zirconate titanate films on metallic substrates by electrophoretic deposition. *Materials Science and Engineering: B*, 116(2):208–214, jan 2005.

[74] R. Maas, M. Koch, N. R. Harris, N. M. White, and A. G. R. Evans. Thick-film printing of PZT onto silicon. *Materials Letters*, 31(1-2):109–112, may 1997.

[75] E. S. Thiele, D. Damjanovic, and N. Setter. Processing and Properties of Screen-Printed Lead Zirconate Titanate Piezoelectric Thick Films on Electroded Silicon. *Journal of the American Ceramic Society*, 84(12):2863–2868, 2001.

[76] N. R. Parikh, J . T. Stephen, M. L. Swanson, and E. R. Myers. Study of diffusion for PZT deposited on Si for non-volatile random-access memory technology. *Materials Research Society Symposium Proceedings*, 200:193–198, 1990.

[77] K. Sreenivas, I. M. Reaney, T. Maeder, N. Setter, C. Jagadish, and R. G. Elliman. Investigation of Pt/Ti bilayer metallization on silicon for ferroelectric thin film integration. *Journal of Applied Physics*, 75:232, 1994.

[78] X. J. Meng, J. G. Cheng, J. L. Sun, H. J. Ye, S. L. Guo, and J. H. Chu. Growth of (100)-oriented LaNiO3 thin films directly on Si substrates by a simple metalorganic decomposition technique for the highly oriented PZT thin films. *Journal of Crystal Growth*, 220(1-2):100–104, nov 2000.

[79] X. J. Meng, Z. X. Ma, J. L. Sun, L. X. Bo, H. J. Ye, S. L. Guo, and J. H. Chu. Highly oriented PbZr0.3Ti0.7O3 thin film on LaNiO3-coated Si substrate derived from a chemical solution technique. *Thin Solid Films*, 372(1-2):271–275, sep 2000.

[80] X. J. Meng, J. L. Sun, J. Yu, G. S. Wang, S. L. Guo, and J. H. Chu. Enhanced fatigue property of PZT thin films using LaNiO 3 thin layer as bottom electrode. *Appl. Phys. A*, 73:323–325, 2001.

[81] H. Miyazaki, T. Goto, Y. Miwa, T. Ohno, H. Suzuki, T. Ota, and M. Takahashi. Preparation and evaluation of LaNiO3 thin film electrode with chemical solution deposition. *Journal of the European Ceramic Society*, 24(6):1005–1008, jan 2004.

[82] S. Thakoor. Enhanced fatigue and retention in ferroelectric thin-film memory capacitors by post-top-electrode anneal treatment ARTICLES YOU MAY BE INTERESTED IN. *Journal of Applied Physics*, 75:5409, 1994.

[83] A. Wold and E. Banks. Rare Earth Nickel Oxides. *Journal of the American Chemical Society*, 70:4911–4913, 1957.

[84] S. Y. Chen and I. W. Chen. Texture Development, Microstructure Evolution, and Crystallization of Chemically Derived PZT Thin Films. *Journal of the American Ceramic Society*, 81(1):97–105, 2005.

[85] D. R. Lide, G. Baysinger, L. I. Berger, R. N. Goldberg, H. V. Kehiaian, K. Kuchitsu, D. L. Roth, and D. Zwillinger. *CRC Handbook of Chemistry and Physics*. CRC Press, Boca Raton, FL, 2005.

[86] J. A. Voigt, D. L. Sipola, B. A. Tuttle, and M. T. Anderson. Nonaqueous Solution Synthesis Process for Preparing Oxide Powders of Lead Zirconate Titanate and Related Materials, 1999.